



# Dynamics of a mesoscale eddy off Cape Ann, Massachusetts in May 2005

Mingshun Jiang<sup>a,\*</sup>, Meng Zhou<sup>a</sup>, Scott P. Libby<sup>b</sup>, Donald M. Anderson<sup>c</sup>

<sup>a</sup> Department of Environmental, Earth and Ocean Sciences, University of Massachusetts Boston, 100 Morrissey Blvd., Boston, MA 02125, USA

<sup>b</sup> Battelle Memorial Institute, 397 Washington St., Duxbury, MA 02332, USA

<sup>c</sup> Woods Hole Oceanographic Institution, Biology Department, Woods Hole, MA 02543, USA

## ARTICLE INFO

### Article history:

Received 10 March 2011

Received in revised form

20 August 2011

Accepted 24 August 2011

Available online 1 September 2011

### Keywords:

Mesoscale eddy

Headland

Cape Ann

Gulf of Maine

Massachusetts Bay

Merrimack River

Freshwater plume

Sub-mesoscale filaments

*Alexandrium fundyense*

Harmful algal bloom

Red tide

## ABSTRACT

Observations and numerical modeling indicate that a mesoscale anti-cyclonic eddy formed south of Cape Ann at the northern entrance of Massachusetts Bay (MB) during May 2005, when large river discharges in the western Gulf of Maine and two strong Nor'easters passing through the regions led to an unprecedented toxic *Alexandrium fundyense* bloom (red tide). Both model results and field measurements suggest that the western Maine Coastal Current separated from Cape Ann around May 7–8, and the eddy formed on around May 10. The eddy was trapped at the formation location for about a week before detaching from the coastline and moving slowly southward on May 17. Both model results and theoretical analysis suggest that the separation of the coastal current from the coast and subsequent eddy formation were initiated at the subsurface by an adverse pressure gradient between Cape Ann and MB due to the higher sea level set up by onshore Ekman transport and higher density in downstream MB. After the formation, the eddy was maintained by the input of vorticity transported by the coastal current from the north, and local vorticity generation around the cape by the horizontal gradients of wind-driven currents, bottom stress, and water density induced by the Merrimack River plume. Observations and model results indicate that the anti-cyclonic eddy significantly changed the pathway of nutrient and biota transport into the coastal areas and enhanced phytoplankton including *Alexandrium* abundances around the perimeter of the eddy and in the western coast of MB.

© 2011 Elsevier Ltd. All rights reserved.

## 1. Introduction

In coastal and open oceans, mesoscale eddies frequently form behind topographic obstacles (e.g., islands, capes, or headlands) which may be detached subsequently from the coastline (eddy shedding) and translated downstream. Normally, this involves two processes, flow separation from the coastline and eddy formation, although a separated flow may re-attach to the coastline and not lead to eddy formation. Numerous numerical and laboratory experiments, and field observations have been conducted to understand these processes in barotropic or stratified oceans (e.g. Signell and Geyer, 1991; Klinger, 1994a,b; Heywood et al., 1996; Cenedese et al., 2005; Dong et al., 2007; Magaldi et al., 2008).

Two dynamic mechanisms for flow separation have been proposed. The first one is that an along-shelf adverse pressure gradient leads to a reverse flow and flow separation (Bachelor, 1967, Signell and Geyer, 1991; Garrett, 1995). This normally occurs for flows with sufficiently high Reynolds number  $Re =$

$UL/v$ , where  $U$ ,  $L$ , and  $v$  are typical current velocity, obstacle length scale, and kinetic viscosity, respectively. As ocean motions are usually fully developed turbulence, kinetic viscosity must be replaced with horizontal turbulent viscosity  $k_H$  for oceanic applications (e.g., Heywood et al., 1996). In shallow coastal areas, bottom friction could become dominant over the lateral friction, and an equivalent Reynolds number  $Re_{ef} = UH^2/k_v R_d$  has been proposed, where  $k_v$ ,  $H$ , and  $R_d$  are vertical turbulent viscosity, water depth, and Rossby radius, respectively (Wolanski et al., 1984; Tomczak, 1988). The second mechanism states that a stratified flow passing a rounded cape would separate from the coast when centrifugal force at the cape lifts the density interface to the surface (Klinger, 1994a). The criterion for this to take place is that the radius of the curvature ( $R_c$ ) is less than the inertial radius  $R_i = U/f$ , where  $f$  is the Coriolis parameter. In both coastal and open oceans, however, several other factors can complicate the dynamics including the shape of the obstacles (e.g. Klinger, 1994b), vertical stratification (Klinger, 1994b; Garrett, 1995; Dong et al., 2007; Magaldi et al., 2008), bottom slope (Signell and Geyer, 1991; Cenedese et al., 2005; Magaldi et al., 2008), and variable flow regimes such as tidal oscillations, and wind forcing and associated Ekman transport (Signell and Geyer, 1991). It has also been suggested that nonlinear advection or hydraulic control

\* Corresponding author. Tel.: +1 617 287 6186.

E-mail address: [mingshun.jiang@umb.edu](mailto:mingshun.jiang@umb.edu) (M. Jiang).

can prevent a flow following the topography and hence lead to flow separation (Jiang, 1995; Dale and Barth, 2001).

It remains unclear what are the critical mechanisms or conditions for a separated flow to evolve into an eddy or eddies. Likely, it will require continuous growth of instability zone over certain period and significant amount of vorticity generation at the same time. However, the dominant factors contributing to the vorticity generation may vary under different situations.

It is well known that eddy formation and transformation behind topographic obstacles have significant ecological and biogeochemical implications in coastal and open oceans (e.g. Wolanski and Hamner, 1988; Dower et al., 1992; Coutis and Middleton, 1999; Hasegawa et al., 2004; Messie et al., 2006). In particular, eddy formation is generally accompanied by strong upwelling in the wake (e.g. Wolanski and Hamner, 1988; Coutis and Middleton, 1999), which transports nutrients from deep waters into the euphotic zone leading to enhanced primary productivity and higher trophic biological activities. Moreover, eddies formed and transported downstream may sustain strong upwelling and nutrient fluxes, and entrap plankton within the vortices (e.g. McGillicuddy et al., 1998, 2007).

Massachusetts Bay (MB) is a semi-enclosed embayment located in the western Gulf of Maine (GOM) (Fig. 1). The dominant coastal current is the western Maine Coastal Current (WMCC), which forms offshore of Penobscot Bay driven by gulf-wide winds, river inputs from the western GOM, and the continuation of the eastern Maine Coastal Current (EMCC) (e.g. Bigelow, 1927; Brooks, 1985; Pettigrew et al., 1998, 2005; Xue et al., 2000; Geyer et al., 2004; Churchill et al., 2005). The WMCC flows southwestward along the New Hampshire (NH) and Massachusetts (MA) coasts. It normally bifurcates around Cape Ann with one branch intruding into MB and the other continuing southward along the eastern flank of Stellwagen Bank toward Great South Channel to join the Georges Bank circulation

(e.g. Bigelow, 1927; Brooks, 1985; Geyer et al., 1992; Lynch et al., 1996). The WMCC is a mostly barotropic current during fall/winter season due to deep mixing, but becomes highly baroclinic during spring time due to strong freshwater discharges including that from the Merrimack River with currents up to 0.7–0.8 m/s (Butman, 1976; Blumberg et al., 1993; Geyer et al., 1992, 2004). When this strong coastal current encounters Cape Ann, a headland with a radius of approximately 8 km, we can expect the flow may separate from the coastline and form mesoscale eddies under favorable conditions.

The WMCC plays a critical role in transporting nutrients and plankton, including zooplankton and harmful algae cells, around the coast and impacting downstream areas (e.g. Franks and Anderson, 1992a,b; Anderson et al., 2005; Keafer et al., 2005; Jiang et al., 2007b). During May 2005, two strong Nor'easter storms swept through the southern New England, following the heavy rain falls and river discharges in late April, which created a strong WMCC and delivered a large amount of nutrients to the coastal waters in the western GOM at the same time. These events led to an unprecedented toxic *Alexandrium fundyense* bloom (red-tide) in the western GOM including MB, due to onshore Ekman transport trapping *Alexandrium* cells in nearshore waters, and southward transport by the WMCC moving the cells downstream (Anderson et al., 2005; Keafer et al., 2005; He et al., 2008). Therefore the dynamics of the WMCC around Cape Ann including the potential of eddy formation is important to the ecosystem and biogeochemical cycles in the surrounding areas, especially MB.

The manuscript is organized as follows. In Section 2, we will briefly describe the numerical model and field surveys for this study. In Section 3, we present evidence of the WMCC separation and eddy formation around Cape Ann during the first strong Nor'easter event in May 2005 and subsequent eddy evolution from in-situ observations and numerical simulation. In Section 4, theoretical analysis and discussion on the flow separation, eddy formation and evolution, and the implications to MB nutrient transport and phytoplankton including the *Alexandrium* blooms will be presented.

## 2. Numerical model and field surveys

### 2.1. Model description

The MB hydrodynamic model is based on the Estuarine, Coastal, Ocean Model (ECOM-si) with Mellor and Yamada 2.5 turbulent closure for the vertical mixing (Blumberg and Mellor, 1987; Blumberg, 1991; Signell et al., 2000). The model domain covers entire MB and a portion of the western GOM with a grid resolution from 200 m in nearshore area to 3 km offshore and 16 vertical sigma levels (Fig. 1). The model is forced with meteorological forcing (heat fluxes and wind stresses), freshwater discharges, tides, and monthly mean temperature, salinity, and surface slope along the open boundary. The short wave radiation is measured at the meteorological tower at Woods Hole Oceanographic Institution (WHOI) and the other heat flux components are estimated using bulk formulation by Weller et al. (1995) based on hourly winds, solar radiation, air temperature, and air pressure measured at the NOAA buoy 44013 as well as relative humidity measured at the Logan Airport. The wind stresses are calculated following the formulation by Large and Pond (1981).

The open boundary conditions for temperature and salinity are based on objective interpolation of CTD data collected by the National Marine Fishery Service, Center of Ocean Observing and Analysis at the University of New Hampshire (UNH), Massachusetts Water Resource Authority (MWRA), and WHOI red-tide surveys during the model year using a software package developed by

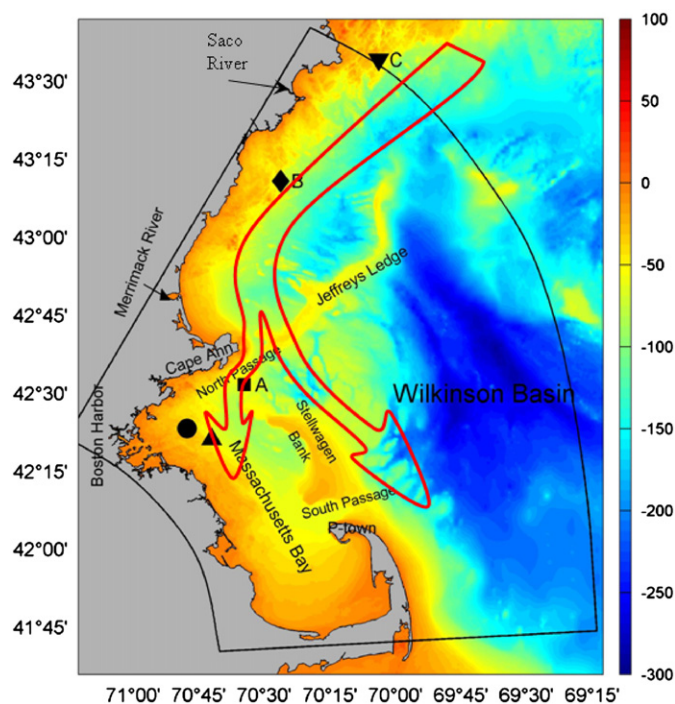


**Fig. 1.** Bathymetry in the western Gulf of Maine and Massachusetts Bay. Also shown are GoMOOS buoys A (square), B (diamond), and C (downward pointing triangle), NOAA buoy 44013 (triangle), and MWRA outfall (black dot). The USGS buoy A is at the outfall site. Black box indicates the model domain. Broad red arrows represent spring circulation pattern of the western Maine Coastal Current and its branching around Cape Ann. (For interpretation of the references to color in this figure legend, the reader is referred to the web version of this article.)

Bedford Institute of Oceanography (Hendry and He, 1996). The surface slope of boundary elevation is estimated from the dynamic height corresponding to the interpolated temperature and salinity with a non-flow layer at 100 m or bottom if shallower. The model also assimilated the temperature, salinity, and currents measured at the Gulf of Maine Ocean Observing System (GoMOOS) buoy C located at the eastern boundary of the domain (Fig. 1). However, currents below 10 m at buoy C were not available for 2005 because the Acoustic Doppler Current Profiler (ADCP) at buoy C was not deployed until December 2007. Therefore the ADCP measurements at the GoMOOS buoy B, about 50 km southwest of buoy C, were used instead. A more detailed description of the hydrodynamic model including the construction of boundary conditions and model calibration can be found in the earlier publications (Signell et al., 2000; HydroQual and Signell, 2001; Jiang and Zhou, 2006).

The initial conditions for 2005 simulation were from the end results of a simulation in 2004. All model outputs of spatial distributions are 12.4 h averaged to remove the semi-diurnal signals. For time series outputs, a 51 h Lanczos filter is applied to remove short-term variations.

## 2.2. Data

In spring 2005, several broad-scale field surveys were conducted in the western GOM by MWRA and WHOI, focused on *Alexandrium* bloom dynamics. In particular, MWRA sponsored a survey covering entire MB in May 9–17, 2005 as a rapid response to the first Nor'easter storm, augmenting the agency's regular monitoring survey earlier in the month. During the same period, a WHOI research team also surveyed the western GOM including MB. Both surveys included CTD casts for temperature, salinity, and chlorophyll measurements, and bottle samples of nutrients and phytoplankton abundances at discrete depths. Similar surveys from both groups were also conducted during the second

storm later in the month. In this manuscript, the hydrographic and phytoplankton data collected during and after the first storm are used to compare with model results, and to investigate the implications of the eddy to nutrient transport and phytoplankton bloom. The temperature, salinity and currents measurements at the two bottom-mounted buoys in northern MB, GoMOOS Buoy A and United State Geographic Survey (USGS) buoy A (Fig. 1), are also used to provide details of the temporal variability at these two locations. Similar to the model outputs, all of the time-series are low-pass filtered with a 51 h Lanczos filter.

## 3. Results

### 3.1. Temperature, salinity, and currents

The hydrodynamic conditions in May 2005 over the western GOM were primarily driven by heavy spring runoff and two Nor'easter storms with surface winds reaching 20 m/s in May 6–10 and May 21–28 (Figs. 2–5; Anderson et al., 2005). During the first storm, winds were predominantly from the north, whereas the winds during the second storm were mostly northeasterly nearly paralleling to the Maine (ME) and NH coastline. During the first storm, local river flows were relatively weak, as compared to the strong river flows following the heavy rainfall during the second storm that greatly enhanced the coastal plume of the WMCC.

Both model and observed temperature at the GoMOOS buoy A showed a general warming trend during this period punctuated by strong vertical mixing of upper layer by the two major storms and the subsequent recovery of stratification within 1–3 days (Fig. 2). Significant freshening occurred before the first storm due to earlier freshwater inputs from the upstream in late April and early May, but the salinity had little trend in May. Between the two storms, there were strong low frequency oscillations in the observed surface temperature and salinity during May 13–21,

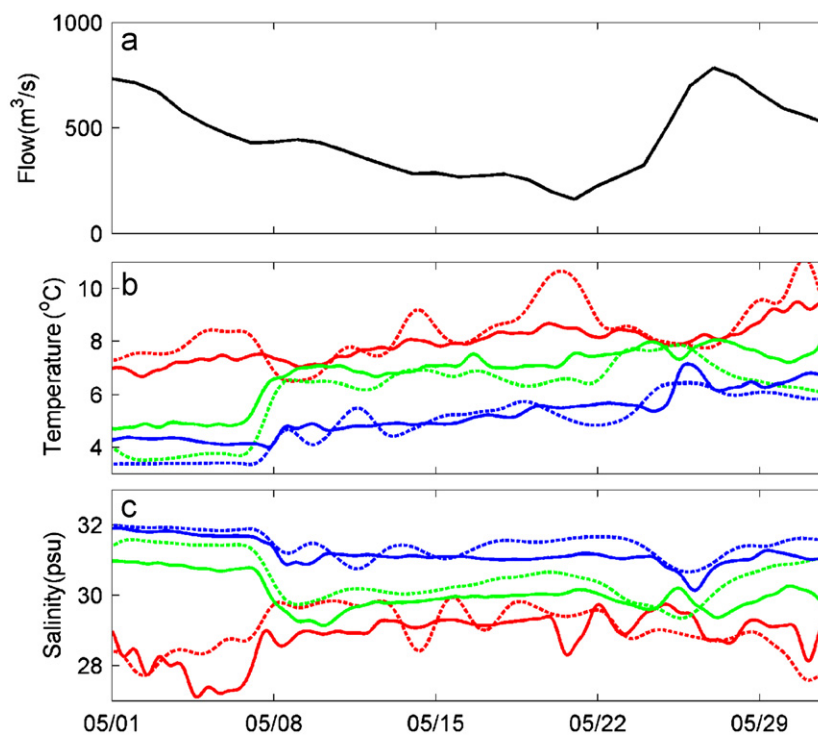


**Fig. 2.** (a) Merrimack River discharge, (b) model (solid lines) and observed (dashed lines) temperature, and (c) model (solid lines) and observed (dashed lines) salinities at the GoMOOS buoy A (red: surface, green: 20 m, blue: 50 m) in May 2005. (For interpretation of the references to color in this figure legend, the reader is referred to the web version of this article.)



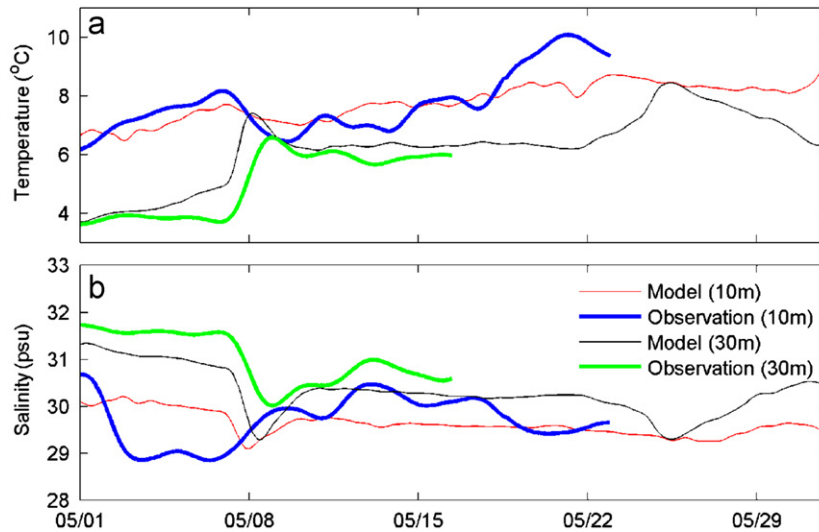


Fig. 3. Model and observed temperature (a) and salinity (b) at 10 m and 30 m at USGS buoy A in May 2005.

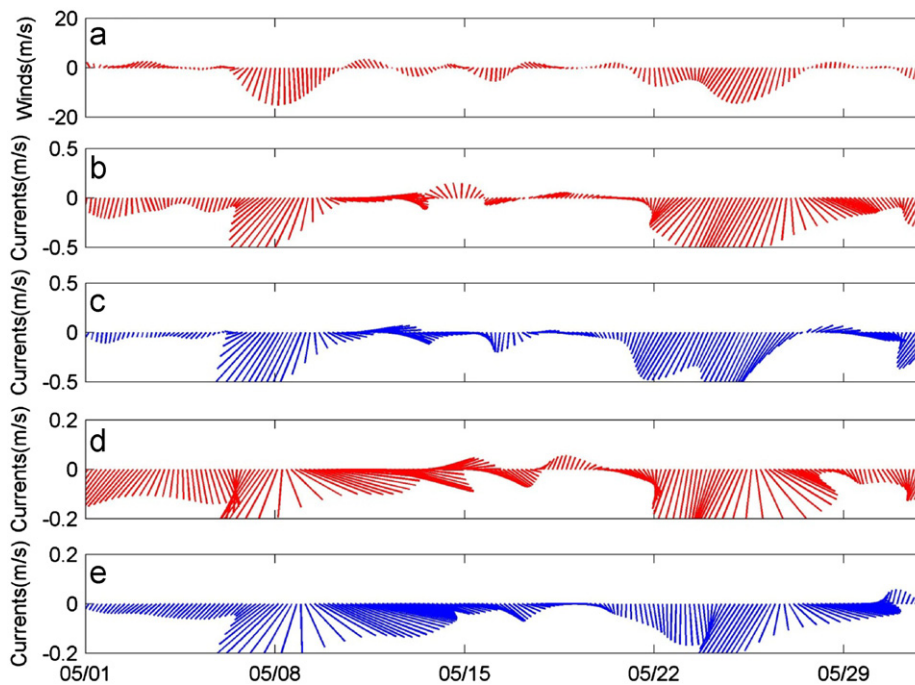


Fig. 4. (a) Surface winds, (b) observed surface currents, (c) model surface currents, (d) observed 20 m currents, and (e) model 20 m currents at the GoMOOS buoy A in May 2005.

which may be due to the movements of the buoyancy front between MB and the GOM (see below). Similar oscillations were also seen in the model results, which occurred a few days later than the observed (May 20–23). In general, the model results compare favorably with measured temperature and salinity, but the model appears to have over-predicted the vertical stratification between the storms and the mixing during the second storm.

Similarly, the model well reproduced observed temperature and salinity at the USGS buoy A including the strong mixing during the two storms that mixed the entire water column at this shallow location (32 m water depth), and the subsequent recovery of stratification (Fig. 3). Both modeled and observed salinities at 10 m and 30 m continued to increase substantially over a period of 2–4 days after both storms, indicating an onshore entrainment of offshore waters.

Both modeled and observed surface and 20 m currents at the GoMOOS buoy A showed a strong response to the storms, with the surface currents increasing from 20 cm/s to more than 70 cm/s (Fig. 4). After the peak of the storms, there was clearly a cyclonic rotation of current vectors when surface winds started to relax and turned northward. Modeled and observed currents at the USGS buoy A also showed a strong response to the two storms but were generally weaker than at the GoMOOS buoy A (Fig. 5). Between the two storms observed currents at 10 m and 20 m were predominantly flowing southward, opposite to the model currents. The reason for this difference will be discussed in Section 3.3.

### 3.2. A mesoscale eddy south of Cape Ann

On May 10, three days after the first storm passing through MB, an anti-cyclonic eddy was formed south of Cape Ann with a

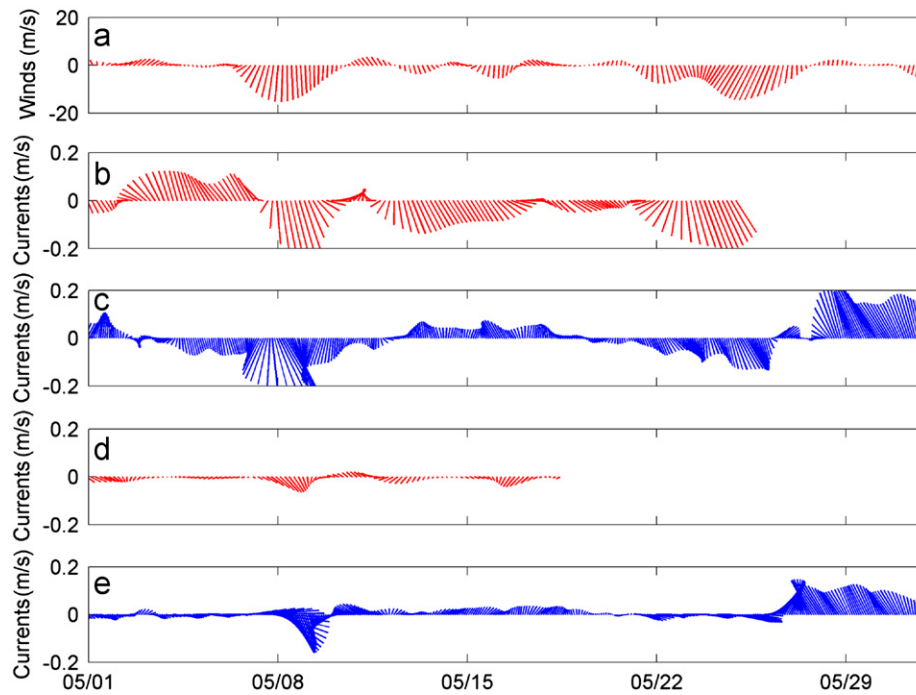


Fig. 5. (a) Surface winds, (b) observed 10 m currents, (c) model 10 m currents, (d) observed 20 m currents, and (e) model 20 m currents at the USGS buoy A in May 2005.

radius of 15 km and currents up to 40 cm/s (Fig. 6). The western edge of the eddy appeared to have touched the MWRA outfall and USGS buoy A. Both the modeled and observed surface salinities showed a low salinity center and a clockwise rotation around the perimeter that entrained offshore high salinity into western MB, which was consistent with the increasing salinity observed at the USGS buoy A during the 2–4 day post-storm period (Fig. 3). Modeled salinity was significantly correlated with the observed salinity ( $r^2=0.33$ ), although model salinity was about 1 psu lower. The eddy blocked the intrusion of GOM water into MB through the North Passage. At the same time, a strong NW to SE salinity front along the eastern flank of the Stellwagen Bank can be seen separating the fresher coastal waters from the GOM offshore waters. Vertically, the eddy had a clear bowl shape with a decreasing eddy radius at depth, as seen in both the modeled and observed vertical distributions of temperature (not shown) and salinity (Fig. 6). Currents along the perimeter were greatest at the surface and decreased to zero at the bottom ( $\sim 50$  m) of the eddy.

On May 17, modeled surface salinity and currents indicated the eddy was about 6–8 km south of the formation location and with much weaker currents, while observed surface salinity showed no sign of the eddy (Fig. 7). The modeled and observed surface salinities, however, showed a strong correlation ( $r^2=0.85$ ). Vertically, modeled salinity also showed a bowl shape eddy structure that is consistent with the observed salinity distributions. Neither observed nor modeled temperature showed a clear bowl shape (not shown).

### 3.3. Formation and evolution of the eddy

The model results provide an integrating view of the eddy formation and evolution. Strong river freshwater inputs prior to the first storm drove a strong coastal current that mostly followed the coastline. Strong northerly winds during the first Nor'easter pushed water shoreward against the coastline and greatly enhanced the coastal current (Figs. 8a and 9b). At the peak of surface winds on May 7, the subsurface coastal current started to

separate from the coast at the tip of Cape Ann, and the separation zone south of Cape Ann grew with time (Figs. 8b and 9b). As a result, currents at the GoMOOS buoy A began to flow southward, instead of southwestward. In the next 2–3 days, northerly winds relaxed, and an eddy formed around May 10 (Figs. 8c–e, and 9c–e).

During May 11–16, the eddy remained attached to the coastline most of the time, but was slowly pushed around by the background currents including Ekman transport (Fig. 8f, g and 9f, g). As the GoMOOS buoy A was located on the northern side of the eddy, modeled currents at this location were dominated by eastward component, consistent with the observed currents (Figs. 4 and 6). In contrast, the currents at the USGS buoy A were sensitive to the eddy's exact location and size. During this period, the western edge of the modeled eddy touched upon the buoy most of the time, and the currents there were generally northward (Fig. 5). However, observed currents at this location were generally southward. This suggests that the actual eddy might be located somewhat eastward or slightly smaller than the modeled one, likely due to the overestimation of vertical stratification in model fields (Figs. 2, 3, and 6). If the modeled eddy was smaller or located further eastward, the direction of modeled currents at this location would have been generally southward because of the dominant northerly winds and river outflow from Boston Harbor.

On May 17, the eddy separated from the coastline and was translated southward in the Stellwagen Basin. The surface portion of the eddy appeared to have disintegrated on May 20, whereas at subsurface the modeled eddy continued to exist until May 22 (not shown), when the second storm arrived at the region. During the life time of the eddy, the eddy formed a strong barrier that blocked the GOM waters from entering MB through the North Passage and hence altered the MB circulation pattern significantly.

The generation and transformation of the eddy were closely associated with the low frequency variability of sea level pattern in MB (Figs. 10 and 11). Before the first storm, sea level gradient in MB was low (Fig. 10a). The strong onshore Ekman transport driven by the first Nor'easter and the subsequent water accumulation in MB led to a strong W–E sea level gradient. As a

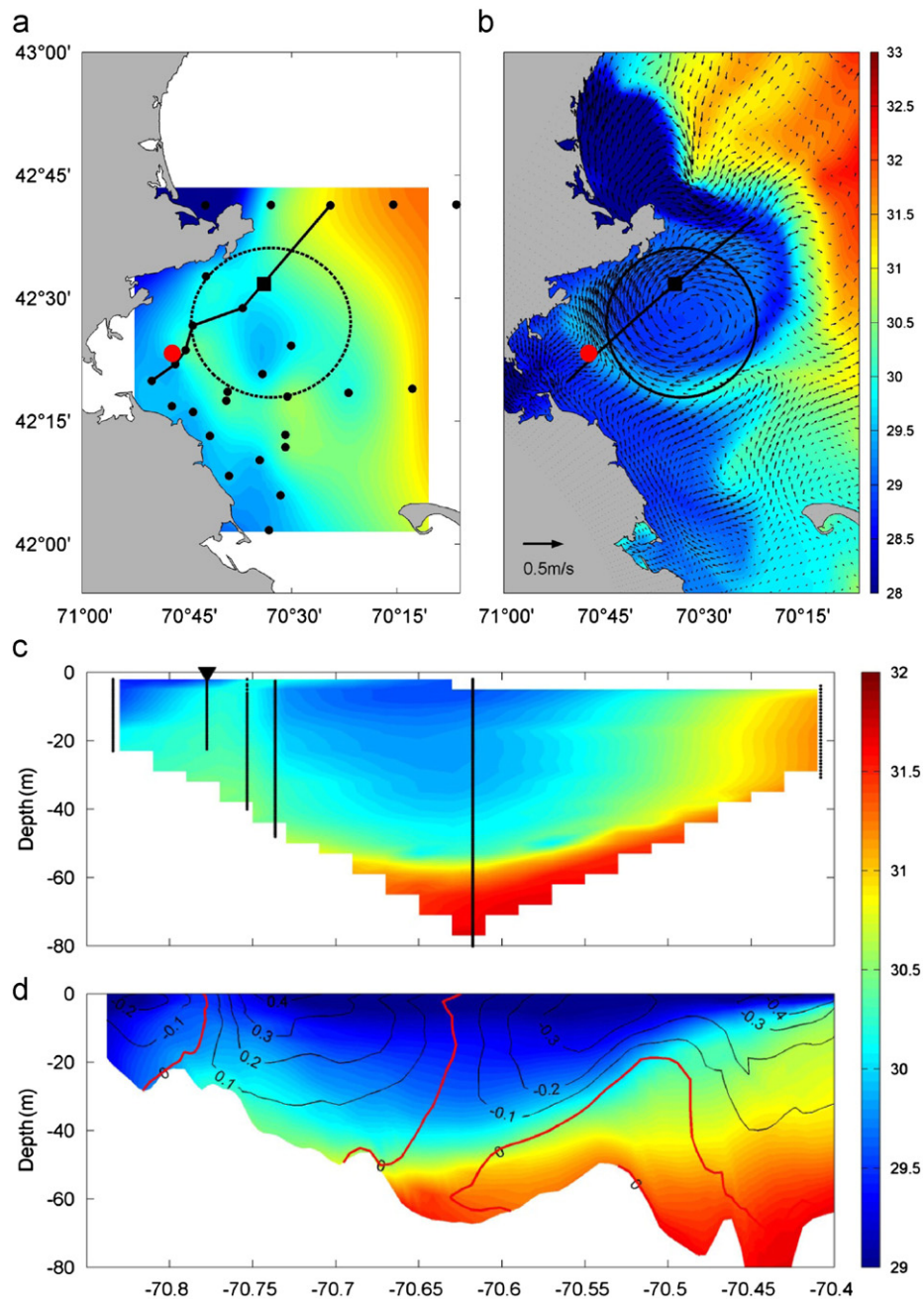


**Fig. 6.** (a) Observed surface salinity in May 10–11, 2005. The sampling stations are marked as black dots. The lines indicate the vertical transects for panel (c). Red dot and black square are the sites of MWRA outfall and GoMOOS buoy A, respectively. Dashed circle indicates the approximate eddy ring from the model. (b) same as (a) but for model surface salinity and currents on May 10, 2005. The line indicates model transect for (d). (c) Observed salinity in May 10–11, 2005 along the SW–NE transect. Black dots indicate the CTD sampling depths. Black downward pointing triangle indicates the location for MWRA outfall and USGS buoy A. (d) Same as (c) but for model salinity and along-shelf (nearly N–S) velocity on May 10, 2005 along the SW–NE transect. (For interpretation of the references to color in this figure legend, the reader is referred to the web version of this article.)

consequence, the sea level at Scituate was markedly higher than those at the upstream locations such as Cape Ann and GoMOOS buoy B (Figs. 10b and 11b). At the peak of this adverse pressure gradient (at the turn of May 7–May 8), coastal current separated from the cape (Figs. 10b and 11b). This is consistent with the suggestion that an adverse pressure gradient is favorable to separation of coastal currents from land (Signell and Geyer, 1991; Garrett, 1995). After the eddy matured, the sea level at Cape Ann followed closely but was slightly lower than that in the upstream area, whereas sea level at Scituate was generally higher than that at Cape Ann except during May 14–15 and May 17–21,

when the eddy was detached from the coast (Fig. 11b). Similar changes of sea level patterns took place during the second storm (Fig. 11), along with a similar mesoscale eddy formed south of Cape Ann (not shown).

#### 3.4. Vorticity generation and sub-mesoscale processes

Strong surface winds and coastal freshwater plume produced significant vorticity, enhancing eddy and coastal jets (Fig. 12). Positive vorticity was generated along the buoyancy front, which was subsequently transported downstream and entrained into



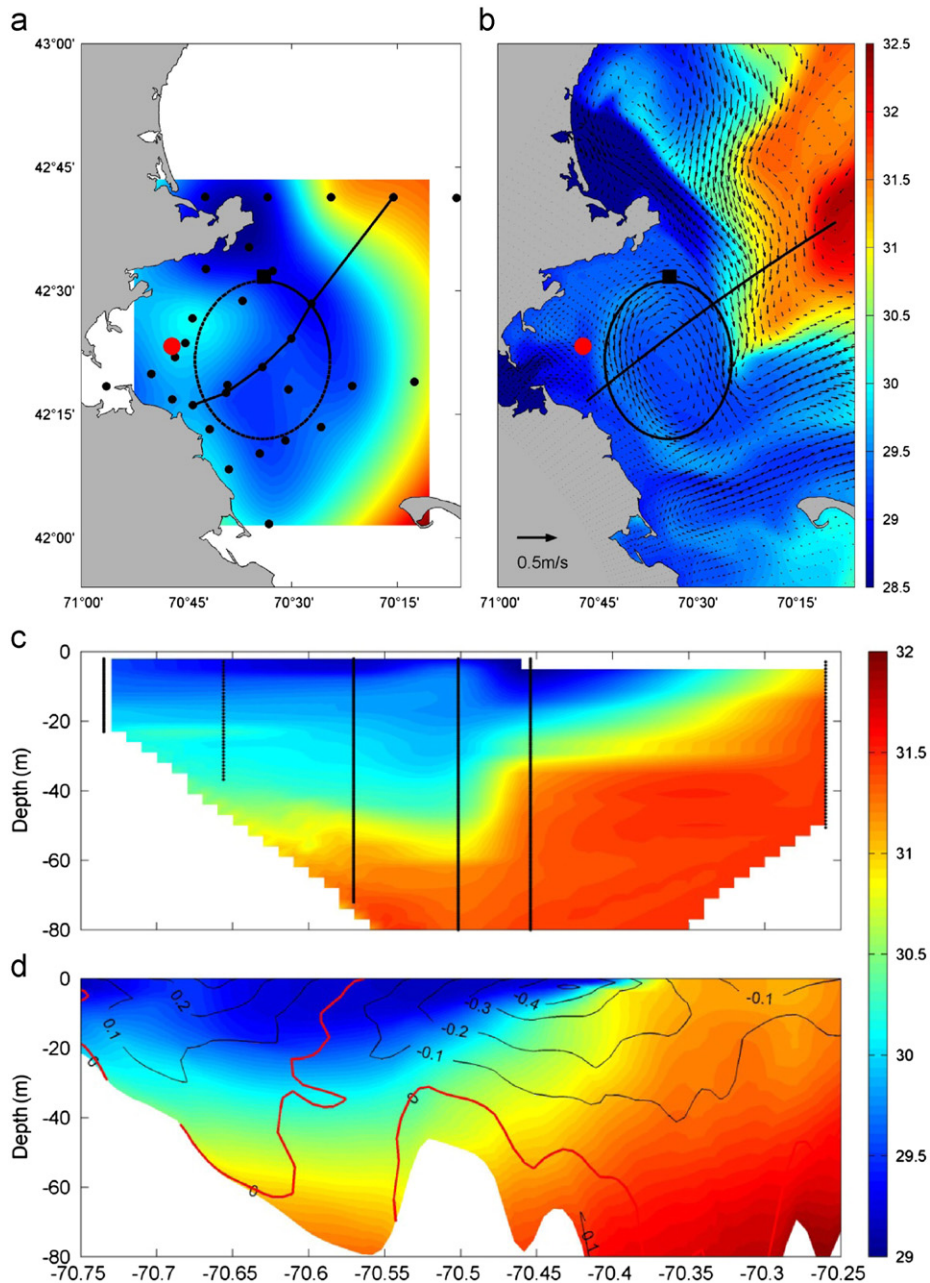


**Fig. 7.** (a) Observed surface salinity on May 17, 2005. The sampling stations are marked as black dots. The lines indicate the vertical transects for panel (c). Red dot and black square are the sites of MWRA outfall and GoMOOS buoy A, respectively. Dashed circle indicates the approximate eddy ring from the model. (b) Same as (a) but for model surface salinity and currents on May 17, 2005. The line indicates model transect for (d). (c) Observed salinity in May 17, 2005 along the SW–NE transect. Black dots indicate the CTD sampling depths. Black downward pointing triangle indicates the location for MWRA outfall and USGS buoy A. (d) Same as (c) but model salinity and along-shelf (nearly N–S) velocity on May 17, 2005 along the SW–NE transects. (For interpretation of the references to color in this figure legend, the reader is referred to the web version of this article.)

the outer perimeter of the eddy. Negative vorticity was generated near the coastline, especially the cape, which gradually developed to form the core of the anti-cyclonic eddy (Fig. 12a, b). After the formation, the eddy was continuously fed with vorticity produced by strong wind forcing, river plume, and coastal jet (Fig. 12c, d). In the core of the eddy the flow was quasi-geostrophic with relatively low Rossby number. Strong nonlinearity, however, existed in the frontal zone and around the perimeter of the eddy with Rossby number  $\sim 1$ , which led to rich sub-mesoscale features with scale of  $\mathcal{O}(1\text{ km})$ . Such sub-mesoscale processes are typically associated with intense upwelling and downwelling that may drive strong vertical nutrient fluxes, and hence are important to phytoplankton bloom and biogeochemical cycle in

the area (e.g. Mahadevan and Tandon, 2006; Lepeyre and Klein, 2006).

### 3.5. Nutrient transport and red-tide bloom

The presence of the eddy south of Cape Ann changed the circulation pattern in MB dramatically, which in turn affected the transport pathways of nutrients and possibly the *Alexandrium* bloom (Fig. 13). Nutrients from upstream in the GOM are typically transported into MB through the North Passage (Fig. 1; Geyer et al., 1992; Jiang et al., 2007b). During May 10–20, however, the eddy (as outlined by the model output in Fig. 13) blocked the entire North Passage such that the water and nutrient inputs from the

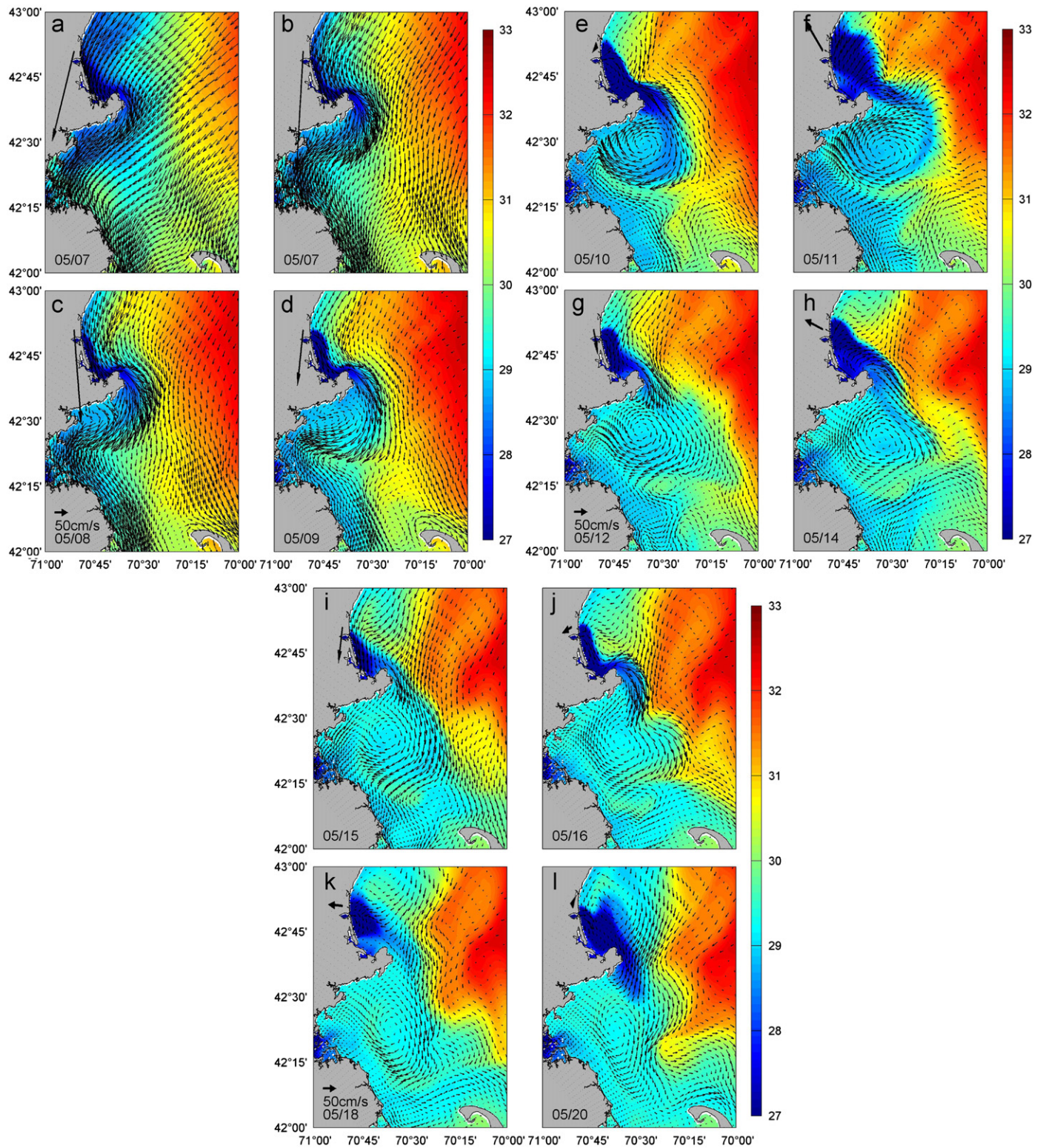


Fig. 8. Model surface salinity and currents in May 7–20, 2005. Black arrow in the top left of each panel indicates the wind speed and direction.

GOM into MB were mainly through eddy entrainment along its southwestern perimeter toward the northwestern coast of MB (Fig. 13a, c). Along the western edge of the eddy, cells of phytoplankton including *Alexandrium* were abundant (Fig. 13b, d), while surface dissolved inorganic nitrogen (DIN) was nearly depleted with DIN concentration being lower than  $2 \mu\text{M}$  (Fig. 13a, c). The average

number of *Alexandrium* cells in western MB was more than doubled over a week period between May 10 and May 17 (Fig. 13b, d), suggesting intense local phytoplankton growth in addition to cell inputs from upstream. The patchy distributions of the DIN concentration and cell abundances also suggest the presence of active sub-mesoscale activities.



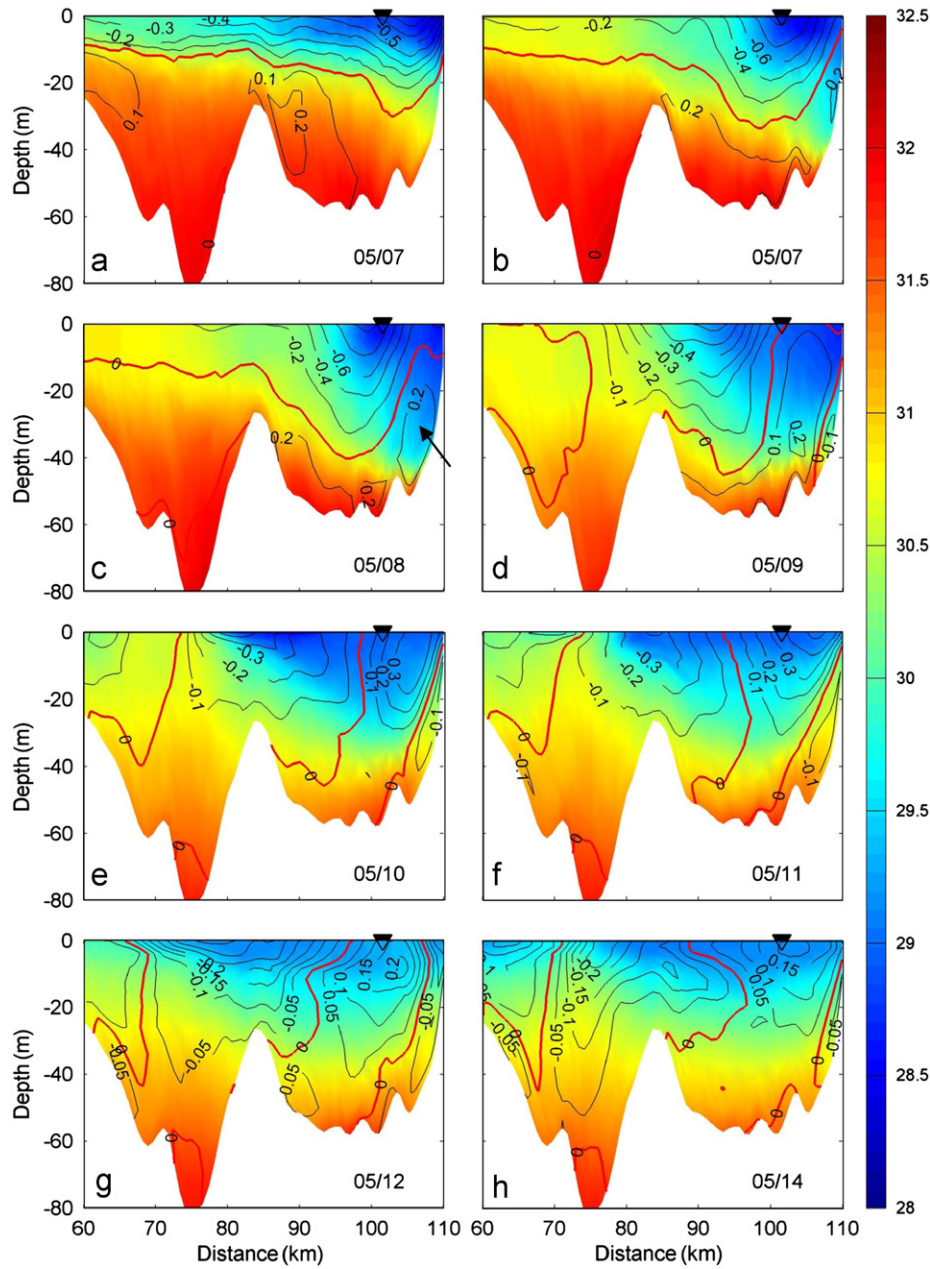


Fig. 9. Salinity and cross-shelf (W–E) velocity along an N–S transect between Provincetown (P-town) and Cape Ann in May 7–14, 2005. The transect passes through GoMOOS buoy A (downward pointing triangle). Black arrow in panel (c) indicates the separation area.

4. Discussion

Complex coastal geometrical setting in the western GOM and multiple forcing present an analytical challenge to understanding the dynamics of flow separation and eddy formation. We will discuss the problem through an idealized framework below. The MB coastline will be simplified as a rectangle open to the south and east, ignoring the influences of Jeffrey Ledges, Stellwagen Bank and the elbow of Cape Cod, and the upstream coastline will be straightened to be parallel to the MB western coast (Fig. 14a). Cape Ann will also be simplified into a rounded headland with an 8 km radius so a polar coordinate can be applied. Vertically, the coastal current will be simplified to a two-layer system with a front that intersects with the oceanic bottom separating the upper layer from a motionless lower layer (Fig. 14b). Following Garrett (1995), the inshore area is called wedge zone, while the area from the intersection to the front is called free zone.

4.1. Separation of the coastal current from Cape Ann

To understand the flow separation, we limit our discussion to the cape area for simplicity (Fig. 14a). The alongshore equation of motion can be written as (see Appendix A)

$$\frac{\partial v_\theta}{\partial t} + v_\theta \frac{\partial v_\theta}{r \partial \theta} + f v_r = -g \frac{\partial \eta}{r \partial \theta} - \frac{g}{h} \int_{-h}^0 \int_{z'}^0 \frac{\partial \rho}{r \partial \theta} dz' dz + \frac{\tau_\theta - \bar{\rho} c_d |v_\theta| v_\theta}{\bar{\rho} h} \quad (1)$$

where  $r, \theta$  are the radial and angular coordinates, respectively,  $v_\theta$  is the alongshore velocity,  $f$  is the Coriolis parameter,  $g$  is the gravity acceleration,  $\eta$  the is sea level,  $\rho$  is the normalized density anomaly ( $=\rho^*/\bar{\rho}$ , where  $\rho^*$  is the density anomaly,  $\bar{\rho}$  is the mean density),  $h$  is the depth of upper layer,  $\tau_\theta$  is the alongshore component of surface wind stress, and  $z'$  and  $z$  are vertical coordinates.

In the case of barotropic flow and zero wind stress, the flow separation occurs where a flow reversal takes place, which

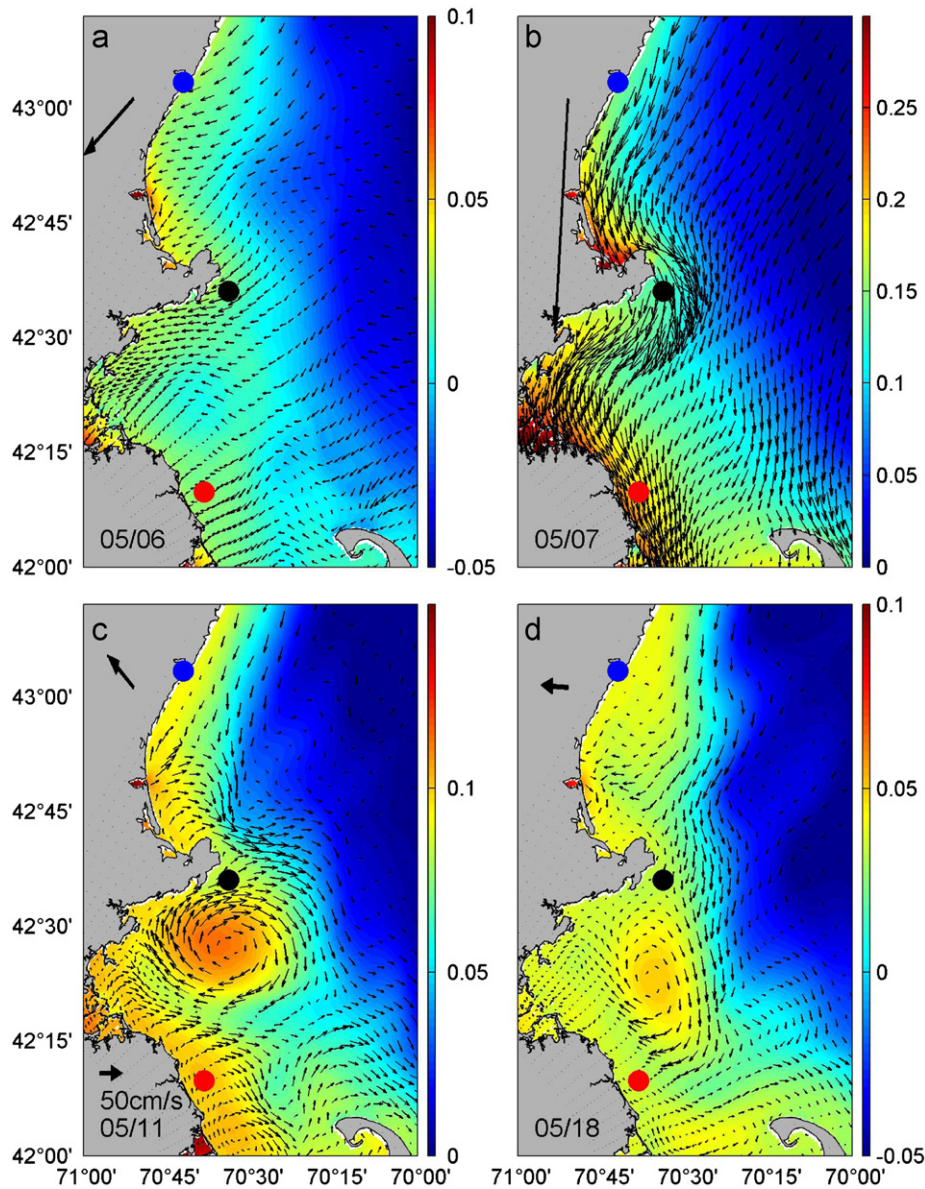


**Fig. 10.** Surface elevation and currents on May 6 (a), May 7 (b), May 11 (c), and May 18 (d). Black arrow in the top left of each panel indicates the wind speed and direction. Three selected locations for time series in Fig. 11 are Scituate (red dot), Cape Ann (black dot), and GoMOOS buoy B (blue dot). (For interpretation of the references to color in this figure legend, the reader is referred to the web version of this article.)

requires that deceleration due to bottom stress exceeds the inertial term (Signell and Geyer, 1991). Based on this criterion, a simple calculation suggests that the flow regime near the cape is on the margin of separation for almost any steady flow (Appendix A), and as such, other factors are critical to the flow separation.

Both surface wind stress and flow baroclinicity will also contribute to the flow acceleration/deceleration and hence affect the flow separation. For northerly winds, the angular component of wind stress  $\tau_\theta = \tau \sin\theta < 0$ , where  $\tau$  is the wind stress (Fig. 14a). Therefore the presence of northerly winds would require greater negative pressure gradient and hence tend to prohibit the flow separation. During the two Nor'easters in May 2005, the prevailing winds were predominantly northerly or northeasterly, which would tend to keep the coastal current attached to the coast while accelerating it. This is consistent with the results that the coastal plume did not separate from the coast when the adverse pressure gradient between Scituate and Cape Ann initially appeared on May 7 (Figs. 9a and 11). The separation only occurred at the turn

of May 7 to May 8, at the peak of negative pressure difference as surface winds started to retreat (Figs. 9 and 11).

Water density increased downstream, especially south of the Merrimack River mouth, as freshwater plume mixed with ambient waters. As a result, the downstream density gradient contributed to the deceleration of the plume and hence increased the likelihood of flow separation, in contrast to the northerly wind effects. At subsurface near thermocline, wind effects were much reduced while the effect of density gradient was increased. Therefore the flow separation was more likely to occur. This is consistent with the modeled separation, which began at subsurface (Fig. 9b, c).

The flow separation can be further understood by a diagnostics of the modeled acceleration/deceleration terms in Eq. (1) along the coastline (Fig. 15). Here we use the line ABC for such a computation, which consists of grid points two-grid away from the nearest land points with smoothing of the sharp topographic turns (Fig. 15a). We note that before the flow separation, both the

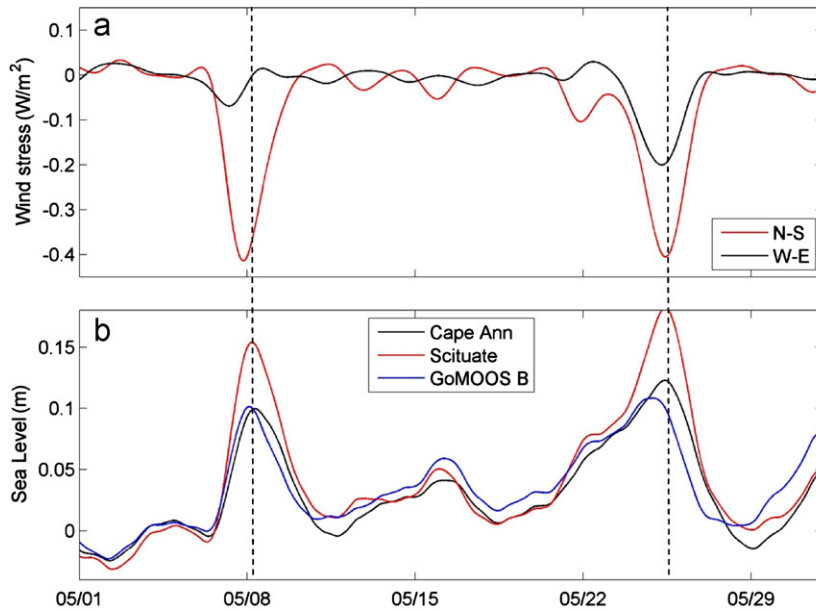


**Fig. 11.** (a) Surface wind stresses at NOAA buoy 44013 and (b) modeled sea levels at Scituate (red), Cape Ann (black), and GoMOOS buoy B (blue) in May 2005 (locations see Fig. 10). Black dashed lines highlight the peaks of sea level at Scituate. (For interpretation of the references to color in this figure legend, the reader is referred to the web version of this article.)

sea level gradient and alongshore velocity near point C were close to zero indicating a stagnant flow regime that was on the margin of flow separation (Fig. 15b, c). Once the sea level gradient became negative, a reverse flow occurred around point C (May 7), which became stronger over time. The accumulated forces on the right hand side of Eq. (1) (surface winds, downstream density gradient, bottom friction, and pressure gradient) between point B and C were presented in Fig. 15d. As discussed above, all major forces were important in the deceleration of the flow from point B to C. As surface wind relaxed on May 7, buoyancy gradient diminished and bottom stress reduced along with reduced currents; however, inverse pressure gradient became increasingly dominant and eventually led to the flow separation at the turn of May 7 to May 8.

Similar phenomena happened during the 2nd storm, the flow separated from the coast on May 21 (not shown), immediately following the setup of a negative pressure gradient between Cape Ann and Scituate (Fig. 11). However, the flow re-attached to the coast during the second phase of the storm, when a strong alongshore wind component accelerated the flow while increasing the negative sea level gradient between Cape Ann and Scituate. The flow separated from the coast again on May 26, when surface winds relaxed and negative pressure gradient became dominant (Fig. 15), and a similar mesoscale eddy formed south of Cape Ann.

In an analysis of a reduced surface layer model, Klinger (1994a) suggested that the centrifugal force of a buoyancy flow rounding a cape may raise the density interface to the surface and hence lead to flow separation. He further suggested that the criterion for that to happen is that  $R_c < R_i$ , the inertial radius. In our case, the parameter  $R_i = U/f$  was in the range of 3–10 km during the storms (current velocity between 30 and 100 cm/s). Since  $R_c = 8$  km, therefore the criterion may be exceeded the criterion. Our results suggested that the upper lifting of the density interface occurred during the flow separation (Fig. 9b), but the thermocline did not reach the surface before the eddy started to form (Fig. 9c–d). One explanation is that in a coastal freshwater plume, the core of the coastal current was 3–10 km away from the coast, and hence the “effective” radius of the cape related to the coastal current was bigger than  $R_c$ .

#### 4.2. Vorticity generation and eddy formation and movement

Vorticity generation is critical to the eddy formation and evolution. Assuming a vertically uniform horizontal density gradient within the surface layer of a plume and weak alongshore depth change as compared to the internal Rossby radius, the non-dimensional vorticity equation can be written as (Appendix A)

$$\frac{d\zeta}{dt} = -\lambda s \frac{\partial \rho}{\partial y} - \sigma \frac{\tau_y s}{h^2} + \kappa \frac{|u_y| u_y s}{h^2} - \varepsilon \frac{1}{h} \frac{\partial |u_y| u_y}{\partial x} \quad (2)$$

where  $\zeta$  is relative vorticity,  $t$ ,  $x$ , and  $y$  are time, cross-shore, and alongshore coordinate, respectively,  $h$  is the depth of upper layer (it is water depth within the wedge zone),  $\rho$  is the normalized water density anomaly,  $s$  is the slope of the thermocline (bottom slope within the wedge zone),  $\tau_y$  is the alongshore component of surface wind stress, and  $u_y$  is the alongshore component of current at the base of the upper layer. The symbols  $\lambda$ ,  $\sigma$ ,  $\kappa$ , and  $\varepsilon$  represent the four non-dimensional parameters characterizing the vorticity generation by vorticity conversion due to baroclinic adjustment, Ekman transport gradient (called Ekman torque hereafter), slope torque and bottom stress torque (Signell and Geyer, 1991), respectively. A simple dimensional analysis suggests that during the two Nor'easter events in May 2005, typical values of the three parameters were  $\lambda = 1$ ,  $\sigma = 0.14$ ,  $\kappa = 0.6$ ,  $\varepsilon = 0.6$  and therefore, all of these four terms may be important to the vorticity generation (Appendix A). The net effect will be dependent on their balance.

The western GOM coastline is generally aligned with the N–S direction. During the two storms, winds were predominantly southward ( $\tau_y < 0$ ), density increased downstream ( $\partial \rho / \partial y < 0$ ) and currents were generally southward ( $u_y < 0$ ). Therefore both the baroclinic vorticity conversion and Ekman torque terms were positive within the wedge zone ( $s > 0$ ), while the slope torque was always negative. The bottom stress torque could be either positive or negative, which tended to reduce the absolute vorticity. The Ekman and slope torques became increasingly important approaching the coast as both of them depended inversely on the square of water depth. Within the free zone ( $s < 0$ ), vorticity conversion and Ekman torque were both negative, whereas the slope torque were generally positive. Thus all these factors



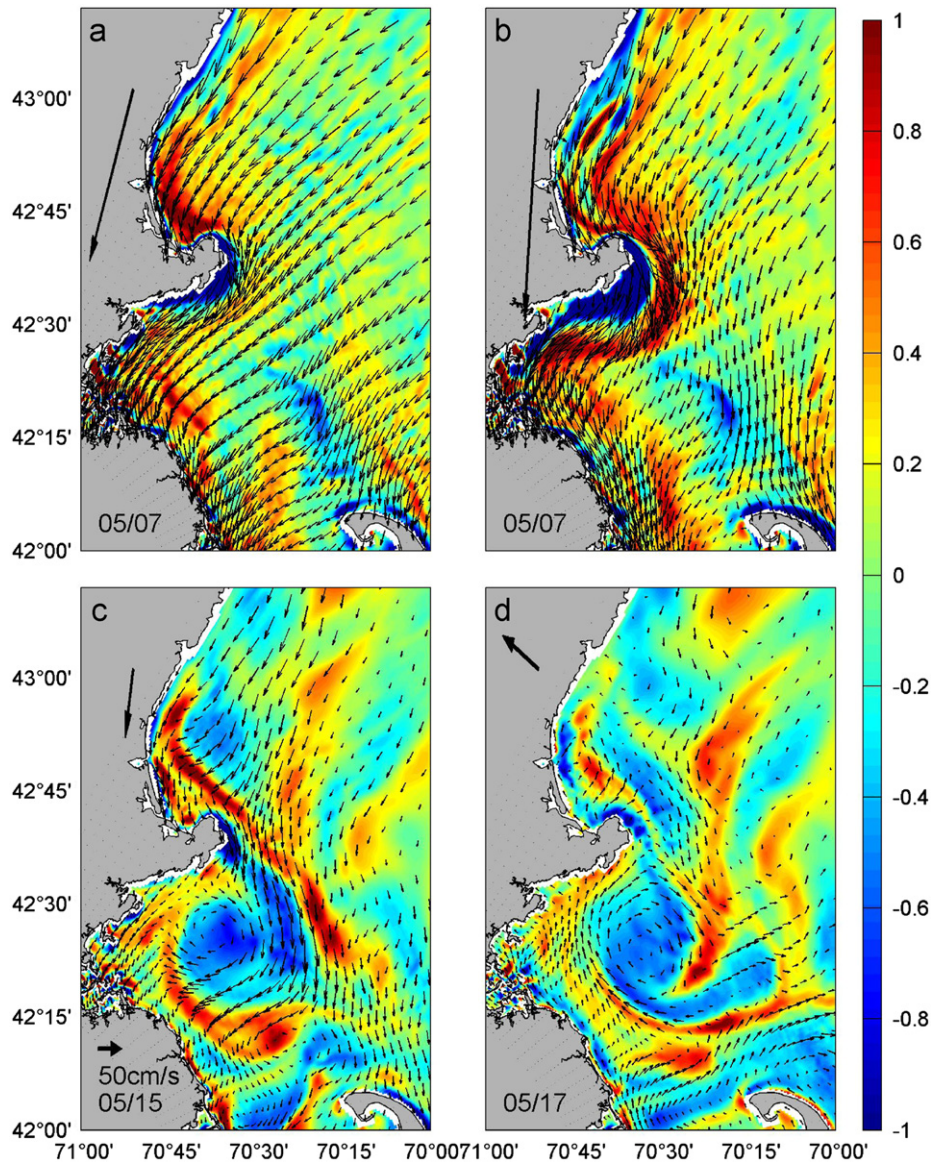


**Fig. 12.** Surface vorticity and currents on first half of May 7 (a), 2nd half of May 7 (b), May 15 (c), and May 17 (d). Black arrow in the top left of each panel indicates the wind speed and direction.

combined together would likely produce significant negative vorticity around the cape. Once the separation occurred, the boundary layer started to grow with the initial negative vorticity from the shore side of the plume. The negative vorticity produced at the separation point and that from the upstream were fed into the boundary layer continuously, which eventually led to the formation of an anti-cyclonic eddy.

The results of this dimensional analysis are largely consistent with a diagnostic computation of vorticity sources based on model results. As an example, the distributions of these terms on May 7 are shown in Fig. 16 along with the surface mixed layer depth. In particular, vorticity conversion due to baroclinic geostrophic adjustment was strong but mostly limited to the buoyancy frontal zone (Fig. 16b). The patchy nature of this term reflected the intense submesoscale upwelling and downwelling along the front. By contrast, surface Ekman torque produced strong positive vorticity within the wedge zone and negative vorticity within the free zone. The slope torque was mainly negative while bottom stress torque was patchy. Due to the strong wind but shallow mixed layer, the surface Ekman torque was stronger than that indicated by the dimensional analysis.

The net result was significant negative vorticity around and south of Cape Ann due to the combination of these terms.

After the eddy formation, these vorticity production and transport processes continued to feed (both positive and negative) vorticity into the edge of the eddy, when the eddy remained attached to the coast for a week or so (Fig. 8e–j). For example, onshore Ekman transport during downwelling winds and the increased cross-shore sea level gradient would enhance coastal current along NH and MA coasts, which in turn would enhance the eddy rotation as well (Fig. 8h, i). Similarly, the Merrimack River plume would contribute to maintain the eddy vorticity (Fig. 8i, j). In the meantime, the eddy was moved by background advection including Ekman transport. An enhanced southward coastal jet would tend to push the eddy away from the coast (Figs. 8i and 12c). In contrast, southerly winds would drive a northward coastal jet that fed into the shoreward edge of the eddy, which would tend to enhance the eddy rotation but also push the eddy against the coast (Fig. 12d). Therefore, both surface winds and upstream currents may play an important role in the entrainment and detachment of the eddy from the cape.

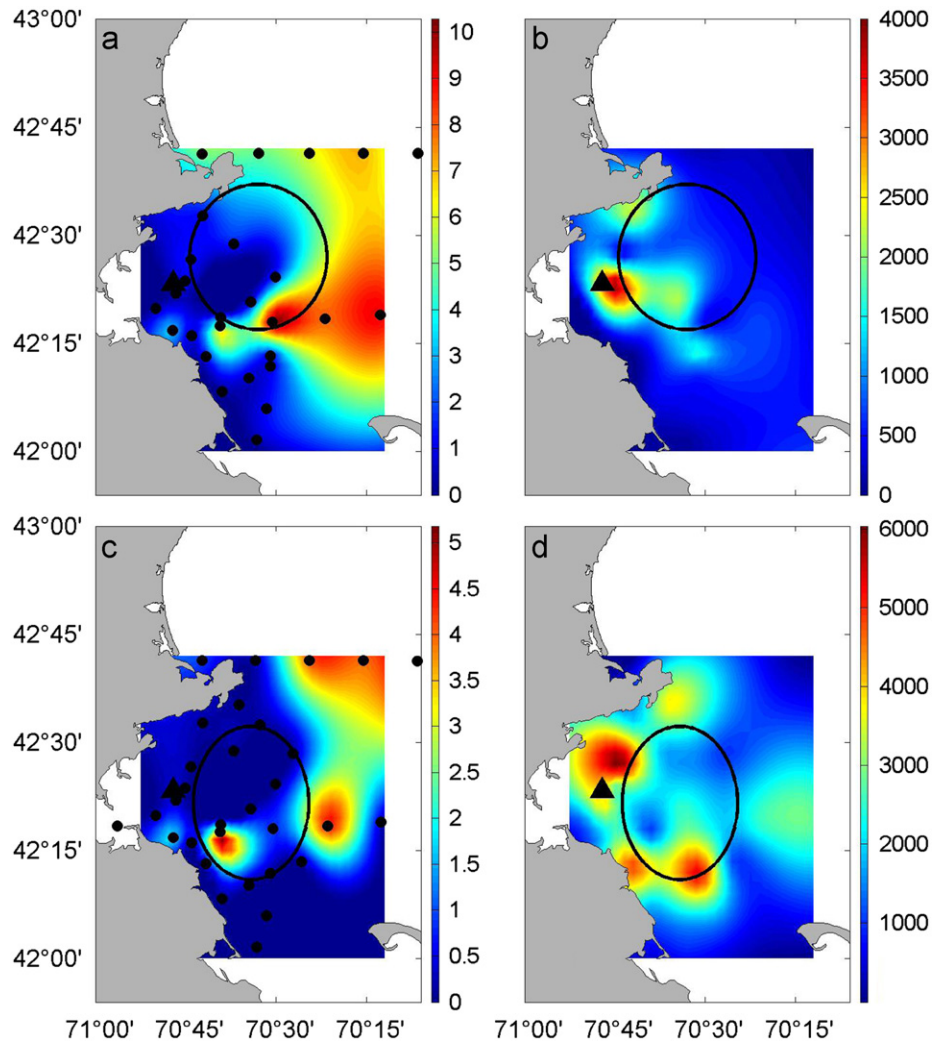


**Fig. 13.** (a) Dissolved inorganic nitrogen (nitrate+ammonium) concentrations and (b) *Alexandrium* cells on May 11, 2005, (c) Dissolved inorganic nitrogen (nitrate+ammonium) concentrations, and (d) *Alexandrium* cells on May 17, 2005. Black dots indicate the sampling stations. Black triangle indicates the location of MWRA outfall and USGS buoy A. Black circles indicate the approximate eddy locations based on model results at the same days (Figs. 6 and 7).

#### 4.3. Implications to MB biogeochemical cycles and ecosystem

The eddy dramatically changed the pathway of the GOM intrusion around Cape Ann and thus MB circulation. As a result, the eddy brought nutrient-rich upstream GOM waters toward the northwestern coastal areas of MB through a mid-bay route crossing the Stellwagen Bank, instead of following the coastline (Figs. 6–8). The eddy might have also interacted with MWRA effluent, brought effluent nutrients toward the north shore fueling phytoplankton blooms, and increased the retention time for nutrients and biota (Figs. 6–8).

The impacts of this nutrient transport on phytoplankton especially *Alexandrium* are suggested in Fig. 13. The 2005 *Alexandrium* bloom started in April 2005 off the western Maine and NH coasts, with the toxic cells subsequently transported southward within the WMCC (Anderson et al., 2005; Keafer et al., 2005). During the first Nor'easter storm in May, massive onshore Ekman transport pushed *Alexandrium* cells into MB (Anderson et al., 2005). After the storm, the altered circulation pattern would retain and enhance the growth of phytoplankton within MB without significant flushing by the coastal current that typically follows the coastline (Geyer et al., 1992), long enough before the second storm arrived to further introduce and entrap cells in MB (Anderson et al., 2005). High cell counts at the stations near the

MWRA outfall during both May 10–11 and May 17 cruises suggest possible impacts of the outfall effluent to the local blooms, but the regional context must be considered in this regard. Specifically, the *Alexandrium* bloom was large and widespread, and patches of cells introduced into MB from upstream waters could explain the high cell densities observed near the outfall. Indeed, using numerical experiments, He et al. (2008) suggested that the MWRA effluent increased the abundance of *Alexandrium* cells in western MB by less than 10%.

As the eddy moved southward, it might also contribute to the transport and growth of phytoplankton including *Alexandrium fundyense* in Cape Cod Bay, potentially explaining the high abundances of this species in Cape Cod Bay observed in May 2005 (Anderson et al., 2005). Overall, the altered circulation pattern was consistent with the *Alexandrium* bloom pattern observed in May 2005.

Similar anti-cyclonic eddies are likely frequently formed around Cape Ann throughout the year, though with variable strength, duration, and evolutionary pattern. For example, model results and observations suggest that an eddy was formed at the similar location after the second Nor'easter in May 2005 and lasted several days (not shown). The existence of such mesoscale eddies may have significant implications to MB biogeochemical cycles and ecosystems. In addition, intense sub-mesoscale upwelling/downwelling around the perimeter of mesoscale eddies may

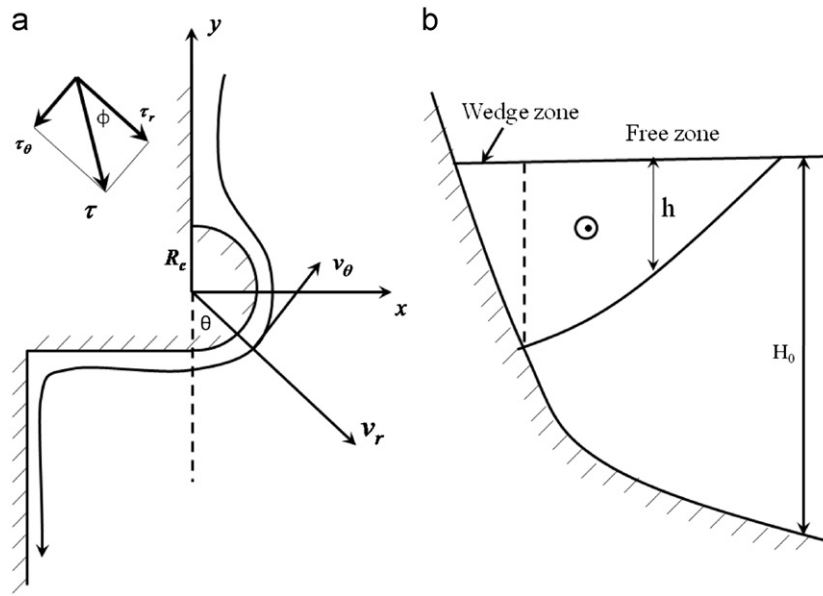


**Fig. 14.** A schematic for the buoyancy flow passing through a cape subject to a wind stress  $\tau$ : (a) plan view and (b) elevation view. Variables  $(x,y)$ , and  $(r,\theta)$  are the Cartesian and polar coordinates, respectively.  $(v_r,v_\theta)$  and  $(\tau_r,\tau_\theta)$  are polar and angular components, respectively, for surface wind stress and currents. The symbols are:  $R_c$ —the radius of the cape,  $h$ —the depth of surface plume, and  $H_0$ —the water depth. Symbol  $\phi$  is the angle of wind vector relative to coastline. For a northerly wind,  $\phi=\theta$ .

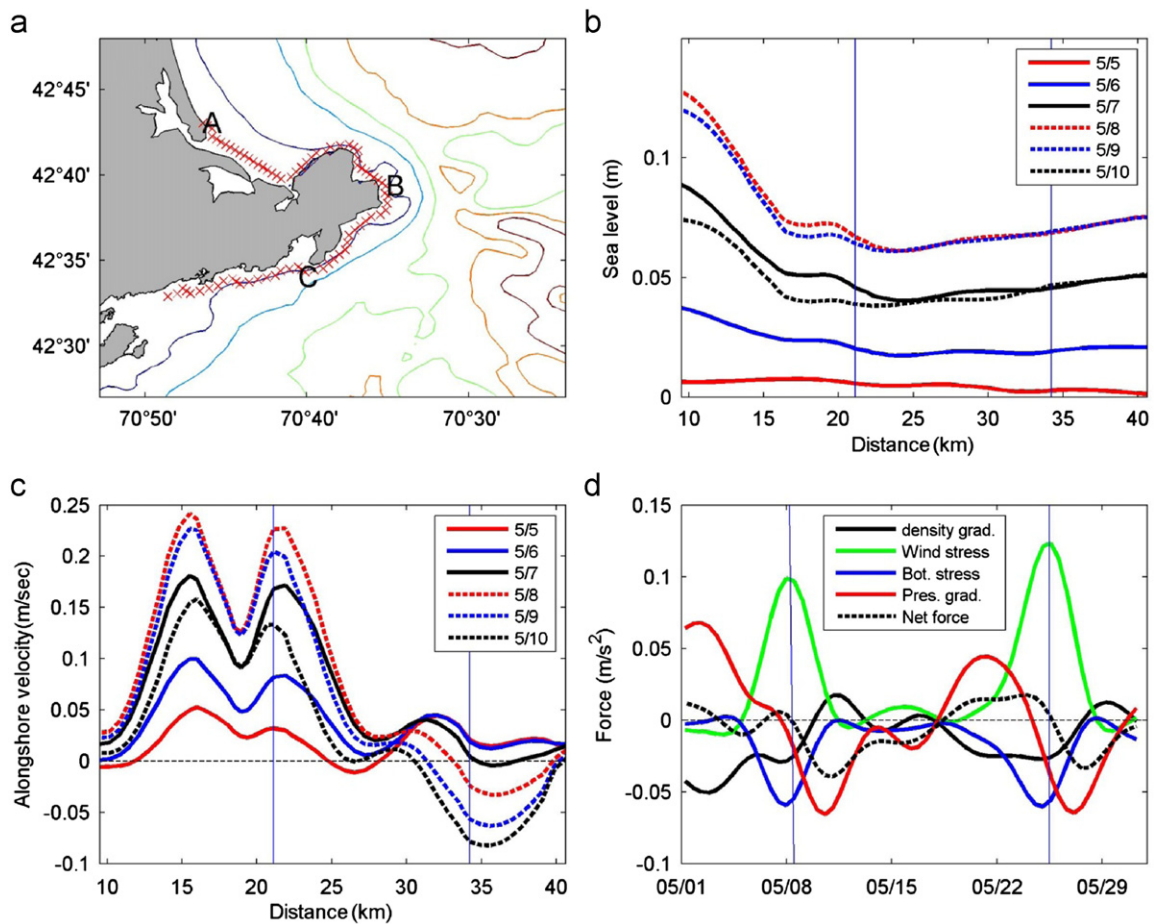


**Fig. 15.** (a) Bathymetry near Cape Ann (depth interval 20 m). Red crosses indicate the transect following the coastline (defined as 2 grid away from the nearest land points) ignoring small sharp turns. A indicates the starting point of the transect. B and C are points used for computation of momentum terms. (b) Surface elevation along the transect on selected dates. Blue thin lines indicate the points B and C. (c) Same as (b) but for alongshore velocity (southward positive). (d) Accumulated momentum terms between points B and C. Blue thin lines highlight the times when net force turned negative. (For interpretation of the references to color in this figure legend, the reader is referred to the web version of this article.)



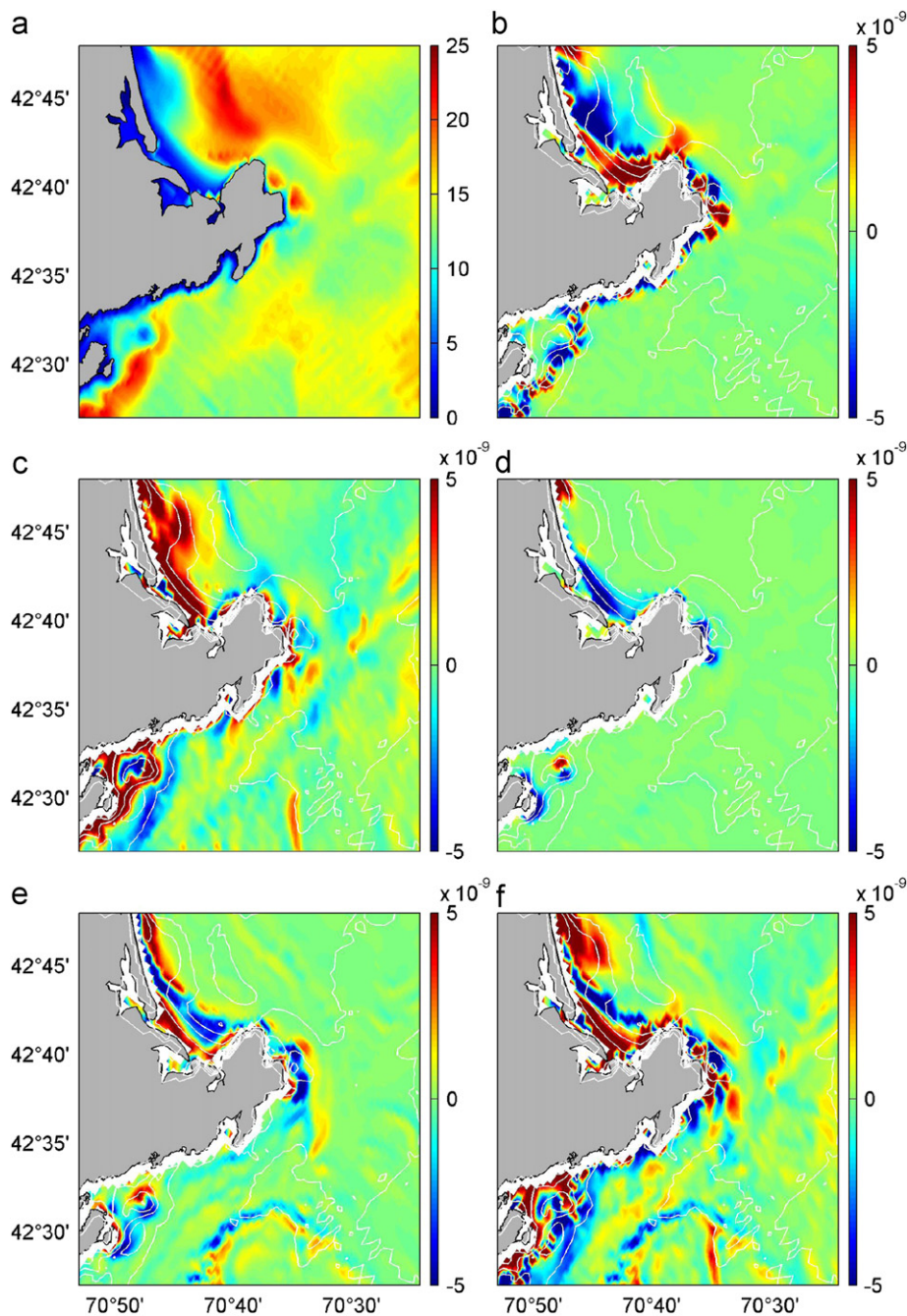


**Fig. 16.** Mixed layer depth and vorticity sources on the first half of May 7, 2005. (a) Model surface mixed layer depth MLD; (b)–(e) vorticity sources due to baroclinic vorticity conversion, surface Ekman torque, slope torque, and bottom stress torque (unit:  $s^{-2}$ ); and (f) net vorticity source.

induce strong vertical nutrient fluxes, although the net effects have yet to be accurately quantified (e.g. Mahadevan and Tandon, 2006; Lepeyre and Klein, 2006). The changing circulation pattern may also impact the transport pathway of phytoplankton, zooplankton, and fish larvae that are important to the MB fishery and whale activities (e.g. Jiang et al., 2007a).

#### Acknowledgments

MJ was partially supported by the MWRA for this work. Observational data are provided by the MWRA, USGS, GoMOOS, WHOI, NMFS, and UNH for model construction and verification. Solar radiation data was provided by Dick Payne at WHOI. We

also thank the Bedford Institute of Oceanography for providing the objective interpolation software. Support for DMA and many of the cruise observations was provided by the GOMTOX project through NOAA Grant NA06NOS4780245. Additional cruise support came from NSF Grant OCE-0430724, DMS-0417769 and NIEHS Grant 1P50-ES01274201 (Woods Hole Center for Oceans and Human Health), and through NOAA ECOHAB Grant NA09NOS4780193. This is ECOHAB contribution number 667.

#### Appendix A

We consider a southward coastal freshwater plume passing through a rounded cape with the coastline on its right (Fig. 14).

The upper layer intersects with the bottom at some distance from the coast. Following Garrett (1995), the inshore area is called wedge zone, while the area between the outcropping point and the bottom intersect point of the thermocline is called free zone. The depth-averaged equation for the upper layer can be written as (e.g. Kowalik and Murty, 1993)

$$\frac{d\vec{u}}{dt} + f\vec{k} \times \vec{u} = -g\nabla\eta - \frac{g}{h} \int_{-h}^{\eta} \int_{z'}^{\eta} \nabla\rho dz' dz + \frac{\vec{\tau} - \vec{\tau}_b}{\bar{\rho}h} \quad (\text{A1})$$

where  $\vec{u}$  is the horizontal current vector,  $f$  is the Coriolis parameter,  $g$  is the gravity acceleration,  $\eta$  is the sea level,  $\rho$  is the normalized density anomaly ( $=\rho^*/\bar{\rho}$ , where  $\rho^*$  is the density anomaly,  $\bar{\rho}$  is the mean density),  $h$  is the depth of upper layer,  $\vec{\tau}$  is the surface wind stress,  $z'$  and  $z$  are vertical coordinates, and  $\vec{\tau}_b$  is the bottom stress at the base of the upper layer. A quadratic form of bottom stress  $\vec{\tau}_b = \bar{\rho}c_d|\vec{u}|\vec{u}$  will be assumed in this study (Large and Pond, 1981). Horizontal mixing term is omitted as it is deemed small compared with other terms. Unlike the uniform density in the upper layer assumed in Garrett's (1995) model, the baroclinic term will remain here in the nearshore area, where freshwater plume evolves through strong mixing and interactions with the bottom topography.

#### A.1. Flow separation

In the cape area, the alongshore equation of motion can be re-written as

$$\frac{\partial v_\theta}{\partial t} + v_\theta \frac{\partial v_\theta}{r\partial\theta} + fv_r = -g \frac{\partial\eta}{r\partial\theta} - \frac{g}{h} \int_{-h}^0 \int_{z'}^0 \frac{\partial\rho}{r\partial\theta} dz' dz + \frac{\tau_\theta - \bar{\rho}c_d|v_\theta|v_\theta}{\bar{\rho}h} \quad (\text{A2})$$

where  $r, \theta$  are the radial and angular coordinates, respectively.

Ignoring the density gradient and surface wind stress, this equation is reduced to that for free barotropic motion. Following the argument by Signell and Geyer (1991) and Garrett (1995), the flow separation occurs where a flow reversal takes place. In a quasi-steady state, this requires the accumulated deceleration due to bottom friction exceeds the inertial term

$$\int_{P1}^{P2} \left| v_\theta \frac{\partial v_\theta}{r\partial\theta} \right| ds < \int_{P1}^{P2} \frac{c_d|v_\theta|v_\theta}{h} ds \quad (\text{A3})$$

where the integration spans from the point along-shore current velocity starting to decrease ( $P1$ ) to the point the current velocity becomes zero ( $P2$ ) (deceleration zone).

This argument is slightly different from that of Signell and Geyer (1991), who did not take into account the fact that the deceleration occurred over a certain distance. Assuming a linear decrease of the alongshore velocity in the deceleration zone, the reversal should occur when

$$R_c < \frac{24H}{c_d\pi^3} \quad (\text{A4})$$

A similar criterion ( $R_{ef}=H/c_dR_c > 1$ ) has also been used for eddy shedding behind an island (e.g., Pingree and Maddock, 1979). Because the thermocline of the freshwater plume intersected with the bottom topography at around 15–25 m before the eddy formation (Fig. 9a), a representative depth  $H=20$  m is chosen. Using typical bottom friction coefficient  $c_d=2.5 \times 10^{-3}$ , Eq. (A4) suggests that the critical radius of the cape  $R_c$  is 8 km, the same as the real radius of the Cape Ann is on the margin of flow separation regime, and hence it is sensitive to other factors such as winds and baroclinic pressure gradient.

#### A.2. Vorticity generation

The vorticity generation near the coastline is better understood in a curvilinear orthogonal coordinate fitting the coastline. Assuming vertically uniform density within the surface layer above the thermocline and spatially uniform winds, and making use of the continuity equation (not shown), the corresponding equation for relative vorticity  $\zeta = \partial v/\partial x - \partial u/\partial y$  (where  $x$  and  $y$  represent the cross-shore and alongshore coordinates and  $u$  and  $v$  are the associated velocity components, respectively) can be written as

$$\frac{d\zeta}{dt} = \frac{\zeta + f}{h} \left[ \frac{\partial\eta}{\partial t} + \vec{u} \cdot \nabla h \right] - \frac{1}{2} g (\nabla h \times \nabla \rho) \cdot \vec{k} + \frac{1}{\bar{\rho}h^2} (\vec{\tau} \times \nabla h) \cdot \vec{k} - \left[ \nabla \times \left( \frac{c_d|\vec{u}|\vec{u}}{h} \right) \right] \cdot \vec{k} \quad (\text{A5})$$

The same equation without buoyancy and wind effects has been derived by Signell and Geyer (1991) for a barotropic study of flow separation and eddy formation. The first term on the right hand side (r.h.s) represents the squeezing and stretching of upper layer. The second term of r.h.s is the baroclinic conversion to vorticity due to geostrophic adjustment. The third term is due to horizontal velocity gradient driven by the Ekman transport. Effectively, a northerly wind working upon an upward tilting of thermocline to the east will produce a negative vorticity. The last term is due to bottom friction, which itself includes slope torque, speed torque and vorticity decay terms (Signell and Geyer, 1991).

We further assume that (a) length-scale of alongshore topographic change ( $L_y$ ) is much larger than the internal Rossby radius, (b) the magnitude of sea level is much smaller than the water depth, and (c) the coastal current is mostly alongshore. During both storms, the flow is strongly nonlinear and therefore we have Rossby number  $R_o = \mathcal{O}(1)$  (see below) and hence  $\mathcal{O}(\zeta) = \mathcal{O}(f)$ . Therefore the first-term on the r.h.s. of Eq. (A5) is an order smaller than the vorticity tendency (l.h.s.). For example, we can estimate that part of the first term relative to vorticity tendency as  $[\zeta/h \partial\eta/\partial t / d\zeta/dt] = [E/H] = \mathcal{O}(10^{-1})$ , where  $E$  is the magnitude of sea level and  $H$  is typical depth. Also we have  $[\zeta/hv \partial h/\partial y / d\zeta/dt] = [R_d/L_y] = \mathcal{O}(10^{-1})$ . Omitting the first term on the r.h.s., the vorticity Eq. (A5) can be simplified as

$$\frac{d\zeta}{dt} = -\frac{1}{2} g (\nabla h \times \nabla \rho) \cdot \vec{k} + \frac{1}{\bar{\rho}h^2} (\vec{\tau} \times \nabla h) \cdot \vec{k} - \left[ \nabla \times \left( \frac{c_d|\vec{u}|\vec{u}}{h} \right) \right] \cdot \vec{k} \quad (\text{A6})$$

Further omitting the terms associated with alongshore topography gradient, we have

$$\frac{d\zeta}{dt} = -\frac{1}{2} g \frac{\partial h \partial \rho}{\partial x \partial y} - \frac{\tau_y}{\bar{\rho}h^2} \frac{\partial h}{\partial x} + c_d \frac{|u_y|u_y}{h^2} \frac{\partial h}{\partial x} - \frac{c_d}{h} \frac{\partial |u_y|u_y}{\partial x} \quad (\text{A7})$$

Here we combine the speed torque and vorticity decay terms into one term, which we call bottom stress torque. A simple dimensional analysis can be performed as follows:  $\zeta = \zeta^* R_d/U$ ,  $x = x^*/R_d$ ,  $y = y^*/R_d$ ,  $t = t^*$ ,  $s = \partial h/\partial x = R \partial h^*/\partial x^*$ , and  $h = h^*/H$ , where for convenience starred and non-starred symbols represent the dimensional and non-dimensional variables, respectively. The internal Rossby radius is  $R_d = \sqrt{g\delta\rho H}/f$  ( $\delta\rho$  is the representative density anomaly across the thermocline). The typical slope of the upper layer is  $S = H/R$ , where  $R$  equals to cross-shore topography length-scale  $R_t$  within the wedge zone and  $R_d$  within the free zone, respectively. The non-dimensional vorticity equation can be

written as

$$\frac{d\zeta}{dt} = -\lambda s \frac{\partial \rho}{\partial y} - \sigma \frac{\tau_y s}{h^2} + \kappa \frac{|u_y| |u_y s|}{h^2} - \varepsilon \frac{1}{h} \frac{\partial |u_y| |u_y}{\partial x} \quad (\text{A8})$$

where  $\lambda = R_d/2R_oR$ ,  $\sigma = \tau R_d/\bar{\rho} f U H R$ ,  $\kappa = c_d R_o^2 R_d^2 / H R$ , and  $\varepsilon = c_d R_o^2 R_d / H$ . Here  $R_o = U / R_d f$  is the Rossby number. A quadratic form of wind stress  $\tau_y = \bar{\rho}_a C_d^a |W| W$  ( $\bar{\rho}_a$  is the air density,  $C_d^a$  is the form drag coefficient for air–sea interface, and  $W$  is the wind speed) will be assumed as well. With strong river inputs especially the Merrimack River in the upstream, the water density around the cape generally increases toward the south, therefore we have  $\partial \rho / \partial y < 0$ , hence the baroclinic term is positive (negative) within the wedge (free) zone. We consider northerly wind case, therefore  $\tau_y < 0$  and the second term of Eq. (A7) is also positive (negative) within the wedge (free) zone. The third term has an opposite sign to the first two terms. The sign of the last term is not immediately clear.

Typical values for these parameters during May 2005 are as follows:  $U = 0.5$  m/s,  $f = 1 \times 10^{-4} \text{ s}^{-1}$ ,  $c_d = 1.2 \times 10^{-3}$ ,  $\bar{\rho}_a = 1.2 \text{ kg/m}^3$ ,  $W = 10$  m/s,  $c_d^a = 1.2 \times 10^{-3}$ ,  $\delta \rho = 5 \text{ kg/m}^3$ , and  $H = 20$  m. Therefore we have  $R_d = 10$  km and  $R_o = 0.5$ . Typical topography length scale is  $R_t = 10$  km and therefore we have  $\lambda = 1/2R_o$ ,  $\sigma = \tau/\bar{\rho} f U H$ ,  $\kappa = c_d R_o^2 R_d / H$ , and  $\varepsilon = \kappa$  for both wedge and free zones. With these typical parameters, we have  $\lambda = 1.0$ ,  $\sigma = 0.14$ ,  $\kappa = 0.6$ ,  $\varepsilon = 0.6$ . Therefore all four terms on the r.h.s. of Eq. A8 could be important to the vorticity generation, although the effect of Ekman torque is generally an order less than the other terms. However, as we approach the coast, water depth becomes much shallower, and the Ekman transport term becomes more important.

## References

- Anderson, D.M., Keafer, B.A., McGillicuddy Jr., D.J., Mickelson, M.J., et al., 2005. Initial observations of the 2005 *Alexandrium fundyense* bloom in southern New England: general patterns and mechanisms. *Deep-Sea Res. II* 52, 2856–2876.
- Bachelor, G.K., 1967. An Introduction to Fluid Dynamics Cambridge University Press, 515 pp.
- Bigelow, H.B., 1927. Physical oceanography of the Gulf of Maine (Part II). *Bull. US Bur. Fish.* 40, 511–1027.
- Blumberg, A.F., 1991. A Primer for ECOM-si, HydroQual, Inc 70 pp.
- Blumberg, A.F., Mellor, G.L., 1987. A description of a three-dimensional coastal ocean circulation model. In: Heaps, N. (Ed.), *Three-Dimensional Coastal Ocean Models*, Coastal and Estuarine Sciences, vol. 4. American Geophysical Union, Washington, DC, pp. 1–6.
- Blumberg, A., Signell, R.P., Jenter, H.L., 1993. Modelling transport processes in the coastal ocean. *J. Mar. Environ. Eng.* 1, 31–52.
- Brooks, D.A., 1985. Vernal circulation in the Gulf of Maine. *J. Geophys. Res.* 90, 4687–4705.
- Butman, B., 1976. Hydrography and low frequency currents associated with the spring runoff in Massachusetts Bay. *Mem. Soc. R. Sci. Liege* 6, 247–275.
- Cenedese, C., Adduce, C., Fratantoni, D., 2005. Laboratory experiments on mesoscale vortices interacting with two islands. *J. Geophys. Res.—Oceans* 110, C09023.
- Churchill, J., Pettigrew, N.R., Signell, R.P., 2005. Structure and variability of the western Maine coastal current. *Deep-Sea Res. II* 52, 2392–2410.
- Coutis, P., Middelton, J., 1999. Flow-topography interaction in the vicinity of an isolated, deep ocean island. *Deep-Sea Res. I* 46, 1633–1652.
- Dale, A.C., Barth, J.A., 2001. The hydraulics of an evolving upwelling jet flowing around a cape. *J. Phys. Oceanogr.* 31, 226–243.
- Dong, C., McWilliams, J.C., Shchepetkin, A.F., 2007. Island wakes in deep water. *J. Phys. Oceanogr.* 37, 962–981.
- Dower, J., Freeland, H., Juniper, K., 1992. A strong biological response to oceanic flow past Cobb seamount. *Deep-Sea Res.* 39A, 1139–1145.
- Franks, P.J.S., Anderson, D.M., 1992a. Toxic phytoplankton blooms in the south-western Gulf of Maine—testing hypotheses of physical control using historical data. *Mar. Biol.* 112 (1), 165–174.
- Franks, P.J.S., Anderson, D.M., 1992b. Toxic phytoplankton blooms in the south-western Gulf of Maine—testing hypotheses of physical control using historical data. *Mar. Biol.* 112, 165–174.
- Garrett, C., 1995. Flow separation in the ocean. In: *Proceedings of the Eighth Aha Huliako'a Hawaiian Winter Workshop*, pp. p119–p124.
- Geyer, W.R., Gardner, G.B., Brown, W.S., Irish, J., Butman, B., Loder, T., Signell, R.P., 1992. Physical Oceanographic Investigation of Massachusetts and Cape Cod Bays, Massachusetts Bay Program, MBP-92-03, 497 pp.
- Geyer, W.R., Signell, R.P., Fong, D.A., Wang, J., Anderson, D.M., Keafer, B.A., 2004. The freshwater transport and dynamics of the western Maine coastal current. *Cont. Shelf Res.* 24, 1339–1357.
- Hasegawa, D., Yamazaki, H., Lueck, R.G., Seuront, L., 2004. How islands stir and fertilize the upper ocean. *Geophys. Res. Lett.* 31, L16303. doi:10.1029/2004GL020143.
- He, R., McGillicuddy, D., Anderson, D., Keafer, B., 2008. Gulf of Maine circulation and harmful algal bloom in Summer 2005: part 2: bio-physical numerical modeling. *J. Geophys. Res.—Oceans* 113, C07040. doi:10.1029/2007JC004602.
- Hendry, R., He, L., 1996. Technical Report on Objective Analysis (OA) Project. Bedford Institute of Oceanography, Dartmouth, Nova Scotia, 105 pp.
- Heywood, K.J., Stevens, D.P., Bigg, G.R., 1996. Eddy formation behind the tropical island of Aldabra. *Deep-Sea Res. I* 43, 555–578.
- HydroQual, Inc., Signell, R.P., 2001. Calibration of the Massachusetts and Cape Cod Bays Hydrodynamic Model: 1998–1999, Boston, Massachusetts Water Resources Authority. Report 2001-12, 170 pp.
- Jiang, M.S., Brown, M.W., Turner, J.T., Kenney, R.D., Mayo, C.A., Zhang, Z., Zhou, M., 2007a. Springtime transport and retention of *Calanus finmarchicus* in Cape Cod Bay and implications to North Atlantic right whale foraging. *Mar. Ecol. Prog. Ser.* 349, 183–197.
- Jiang, M.S., Zhou, M., Libby, S., Hunt, C., 2007b. Influences of the Gulf of Maine intrusion on the Massachusetts Bay spring bloom: a comparison between 1998 and 2000. *Cont. Shelf Res.* 27 (19), 2465–2485.
- Jiang, M., Zhou, M., 2006. The Massachusetts and Cape Cod Bays Hydrodynamic Model: 2002–2004 Simulation. Boston, Massachusetts Water Resources Authority. Report 2006-12, 128 pp.
- Jiang, X., 1995. Flow Separation by Interfacial Upwelling in the Coastal Ocean. M.S. Thesis. School of Earth and Ocean Sciences, University of Victoria, 55 pp.
- Keafer, B.A., Churchill, J.H., McGillicuddy, D.J., Anderson, D.M., 2005. Bloom development and transport of toxic *Alexandrium fundyense* populations within a coastal plume in the Gulf of Maine. *Deep-Sea Res. II* 52 (19–21), 2674–2697.
- Klinger, B.A., 1994a. Inviscid current separation from rounded Capes. *J. Phys. Oceanogr.* 24, 1805–1811.
- Klinger, B.A., 1994b. Baroclinic eddy generation at sharp corner in a rotating system. *J. Geophys. Res.* 99 (C5), 12515–12531.
- Kowalik, Z., Murty, T.S., 1993. Numerical Modeling of Ocean Dynamics World Scientific Publishing, Singapore, 481 pp.
- Lepeyre, G., Klein, P., 2006. Impact of the small-scale elongated filaments on the oceanic vertical pump. *J. Mar. Res.* 64, 835–851.
- Large, W.G., Pond, S., 1981. Open ocean momentum flux measurements in moderate to strong winds. *J. Phys. Oceanogr.* 11, 324–336.
- Lynch, D.R., Naimie, C.E., Werner, F.E., 1996. Comprehensive coastal circulation model with application to the Gulf of Maine. *Cont. Shelf Res.* 12, 37–64.
- Magaldi, M.G.T.M., Ozgokmen, A., Griffa, E.P., Chassignet, M., Iskandarani, Peters, H., 2008. Turbulent flow regimes behind a coastal cape in a stratified and rotating environment. *Ocean Modelling* 25, 65–82.
- Mahadevan, A., Tandon, A., 2006. An analysis of mechanisms for submesoscale vertical motion at ocean fronts. *Ocean Modelling* 14, 241–256.
- McGillicuddy, D.J., Robinson, A.R., Siegel, D.A., Jannasch, H.W., Johnson, R., et al., 1998. Influence of mesoscale eddies on new production in the Sargasso Sea. *Nature* 394, 263–266.
- McGillicuddy, D.J., Anderson, L., Bates, N., Bibby, T., Buesseler, K.O., et al., 2007. Eddy/wind interactions stimulate extraordinary mid-ocean plankton blooms. *Science* 316, 1021–1026.
- Messie, M., Radenac, M.H., Lefevre, J., Marchesiello, P., 2006. Chlorophyll bloom in the western Pacific at the end of the 1997–1998 El Niño: the role of the Kiribati Islands. *Geophys. Res. Lett.* 33, L14601. doi:10.1029/2006GL026033.
- Pettigrew, N.R., Townsend, D.W., Xue, H.J., Walling, J.P., Brickley, P.J., Hetland, R.D., 1998. Observations of the Eastern Maine Coastal Current and its offshore extensions in 1994. *J. Geophys. Res.—Oceans* 103 (C13), 30623–30639.
- Pettigrew, N.R., Churchill, J.H., Janzen, C.D., et al., 2005. The kinematic and hydrographic structure of the Gulf of Maine coastal current. *Deep-Sea Res. II* 52, 2369–2391.
- Pingree, R.D., Maddock, L., 1979. The tidal physics of headland flows and offshore tidal bank formation. *Mar. Geol.* 32, 269–289.
- Signell, R.P., Geyer, W.R., 1991. Transient eddy formation around headlands. *J. Geophys. Res.* 96, 2561–2575.
- Signell, R.P., Jenter, H.L., Blumberg, A.F., 2000. Predicting the physical effects of relocating Boston's sewage outfall. *Estuar. Coast. Shelf Sci.* 50, 59–72.
- Tomczak, M., 1988. Island wakes in deep and shallow water. *J. Geophys. Res.—Oceans* 93, 5153–5154.
- Weller, R., Rudnick, D., Brink, N.J., 1995. Meteorological variability and air–sea fluxes at a closely spaced array of surface moorings. *J. Geophys. Res.—Oceans* 100, 4867–4883.
- Wolanski, E., Hamner, W.M., 1988. Topographically controlled fronts in the ocean and their biological influence. *Science* 241, 177–182.
- Wolanski, E., Imberger, J., Heron, M.L., 1984. Island wakes in shallow coastal waters. *J. Geophys. Res.* 89, 10553–10569.
- Xue, H.J., Chai, F., Pettigrew, N.R., 2000. A model study of the seasonal circulation in the Gulf of Maine. *J. Phys. Oceanogr.* 30, 1111–1135.